July 2016

EVALUATING FEATURES FOR BROAD SPECIES BASED CLASSIFICATION OF BIRD OBSERVATIONS USING DUAL-POLARIZED DOPPLER WEATHER RADAR

Sheila Werth
University of Massachusetts Amherst

EVALUATING FEATURES FOR BROAD SPECIES BASED CLASSIFICATION OF BIRD OBSERVATIONS USING DUAL-POLARIZED DOPPLER WEATHER RADAR

A Thesis Presented

by

SHEILA P. WERTH

Submitted to the Graduate School of the
University of Massachusetts Amherst in partial fulfillment
of the requirements for the degree of

MASTER OF SCIENCE IN ELECTRICAL AND COMPUTER ENGINEERING

May 2016

Electrical and Computer Engineering

EVALUATING FEATURES FOR BROAD SPECIES BASED CLASSIFICATION OF BIRD OBSERVATIONS USING DUAL-POLARIZED DOPPLER WEATHER RADAR

A Thesis Presented

by

SHEILA P. WERTH

Approved as to style and content by:

_____
Stephen Frasier, Chair

_____
Ramakrishna Janaswamy, Member

_____
Daniel Sheldon, Member

_____
C. V. Hollot, Department Head
Electrical and Computer Engineering

To my parents.

ACKNOWLEDGMENTS

Many people generously provided critical mentorship on this project. I'd like to acknowledge Prof. Stephen Frasier for his guidance and for making laboratory resources available. Prof. Ramakrishna Janaswamy, for technical insight, inspiring modeling ideas, and a shared passion for birds. Prof. Sheldon for his patience, availability, and valuable suggestions.

Many thanks to my MIRSL colleagues: for their support, friendship, and feedback. To Tom Hartley for sharing a tremendous knowledge base, assisting with hardware, and for managing the lab with incredible grace. To Erik Knapp, for his interest and thought provoking discussions on my project. To Dr. Krzysztof Orzel, for his friendship, energy, and technical prowess.

Finally, I owe tremendous gratitude to Roy Sivley of the MITRE Cooperation, for hours of thoughtful discussion and feedback on feature engineering and classification.

ABSTRACT

EVALUATING FEATURES FOR BROAD SPECIES BASED CLASSIFICATION OF BIRD OBSERVATIONS USING DUAL-POLARIZED DOPPLER WEATHER RADAR

MAY 2016

SHEILA P. WERTH

B.Sc., WORCESTER POLYTECHNIC INSTITUTE, WORCESTER

M.S.E.C.E.., UNIVERSITY OF MASSACHUSETTS AMHERST

Directed by: Professor Stephen J. Frasier

Wind energy is one of the fastest-growing segments of the world energy market; however, wind energy facilities can have detrimental effects on wildlife, especially birds and bats. The ability to monitor vulnerable species in the vicinity of proposed wind sites could enable site selection that favors more vulnerable species, but current monitoring tools lack this classification capability. This work analyzes polarimetric and Doppler measurements of migrating birds for species based variation.

A novel two stage feature extraction technique was developed to enable comparison between birds. Stage one involves mapping time changing radar measurements to the birds behavioral state in time (i.e. flapping and gliding); stage two uses this behavioral state information to produce temporal and statistical features that describe the frequency and appearance of these different behavioral states.

General trends of temporal features (ex. wing-beat frequency) in the dataset match Ecological literature and validate the feature extraction approach. Preliminary clustering

of bird detection data suggests possible species based subgroups of targets, although a larger dataset is needed for further validation.

TABLE OF CONTENTS

Page

LIST OF TABLES

Table Page

LIST OF FIGURES

Figure Page

CHAPTER 1

INTRODUCTION

Wind energy is one of the fastest-growing segments of the world energy market, offering a clean and abundant source of electricity to meet growing demands. However, wind energy facilities can have detrimental effects on wildlife, especially birds and bats, exposing them to increased mortality through turbine collisions and altering behavior, habitat use, and movement patterns. Under federal laws, regulatory agencies, such as the bureau of Ocean Energy Management (BOEM) and the U.S. Fish and Wildlife Service (USFWS), have an obligation to protect wildlife populations affected by wind facilities.

The anticipated expansion of both land-based and offshore wind installations has generated increasing concern about cumulative environmental consequences, particularly to wildlife. Monitoring tools are needed to better quantify the potential and ongoing impacts of wind installations, either for site development or for compliance with federal wildlife regulations. Mapping the dominant flight paths of migratory species is critical to inform the selection of minimally harmful locations for land-based and offshore wind farms.

A variety of techniques have been employed to map bird and bat traffic in the viscidity of prospective sites. Thermal imaging technology detects heat radiating from birds at distances as great as 3km [1], although targets are not resolved in range. Acoustic methods involve recording sounds in a region of interest and associating recordings with calls of certain species. This technique is vulnerable to noise sources in the environment, like wind or waves. Like thermal cameras, a major limitation of acoustic monitoring is

the inability to resolve the altitude and range of a target [1]. This information is of critical importance to determine which organisms are at rotor swept heights.

Unlike conventional camera and acoustic based methods, radar can detect birds at great distances, providing resolved range information. Avian monitoring systems based on marine navigation radar are often used to quantify bird and bat migration near both potential and established wind sites because these radars are relatively inexpensive, easy to maintain, and can be easily modified. However, these instruments lack polarization and some Doppler capabilities, therefore lacking in target discriminator information. Even with more sophisticated systems, the ability to distinguish between bats and different varieties of bird is still not practically achieved. The capability to identify different broad categories of biological scatterers could enable site selection that favors more vulnerable species, such as bats and raptors.

The potential for exploiting meteorological radar for avian studies has been explored by [2]. Radar scattering properties of biological scatterers have been studied using dual polarized weather radars [3] [4] [5] [6] [7], in the S-band range and primarily for the purpose of preventing undesired contamination of meteorological data. More recently, research has reviewed azimuthal dependencies of polarimetric properties in echoes from bio-scatter for the purpose of ecological research [8]. These properties were found to not only vary by azimuthal orientation, but also by species, although classification utility was not explored.

This thesis extends previous work by exploring the value of polarimetric and Doppler radar measurements for species based classification. In order to do this, the UMass X-Pol weather radar was used to collect observations of migrating birds. A two-

step feature extraction technique was used to enable meaningful comparison between birds using the radar measurements. Step one involves mapping time-changing radar measurements to different behavioral states (i.e. flapping, gliding), resulting in a behavioral state that is known at each point in time. When the behavioral state of a bird is known, additional features may be extracted that further describe the bird. These features may be (1) temporal in nature, describing the order and frequency of the bird's different behavioral states, or (2) statistical, describing the way a bird generally looks to the radar during each behavioral state, in terms of the original radar measurements. Clustering of these features reveals suspected species-based groups of observations, although a larger dataset is needed to confirm these findings.

Chapter 2 of this thesis provides a brief introduction to dual-polarized radar, previous polarimetric studies of birds, and the radar hardware used to collect data for this study. Detection algorithms and methods used to generate polarimetric and Doppler metrics will be covered in Chapter 3. Chapter 4 will describe the two stage feature extraction approach. Finally, preliminary clustering results, produced using these features, are presented in Chapter 5, followed by a thesis summary in Chapter 6.

CHAPTER 2

BACKGROUND

Although species based variation in radar data has yet to be thoroughly studied, radar signatures of birds have been reviewed using polarimetric radar [3] [4] [6] [5]. Section 2.1 will outline the standard products produced by dual polarized radar and Section 2.2 will cover previous studies of avian targets. The radar hardware and data collection procedure are reviewed in Section 2.3.

2.1 Dual Polarized Radar Products

A traditional radar system measures echo power P_r at a single electromagnetic polarization. Return power is related to the cross section, σ, of a point target through the following formula:

$$\sigma = \frac{64\pi^3 P_r R^4}{G^2 \lambda^2 P_t} \ [cm^2] \tag{2.1}$$

Here, G is antenna gain, λ denotes wavelength, P_t is transmit power, and R is the range from the radar to the target. Target cross section is a function of its physical size and target azimuthal orientation with respect to the radar. When the target is a single bird, cross section will vary as the bird flaps and changes its body shape. When many birds are present within a single pulse volume, reflectivity Z is proportional to echo power and measures the size and or density of birds within the illuminated volume.

Unlike conventional radar systems, dual polarized radars transmit and receive energy at two orthogonal polarizations, as shown in Figure 1. Measurements from both

polarization yield standard meteorological polarimetric products, including differential reflectivity Z_{dr}, correlation coefficient ρ_{hv}, and differential phase ψ_{dp}. These metrics describe target shape and aspect ratio at different points in time. For a bird, shape and aspect ratio vary by species and also as it moves its body in flight.

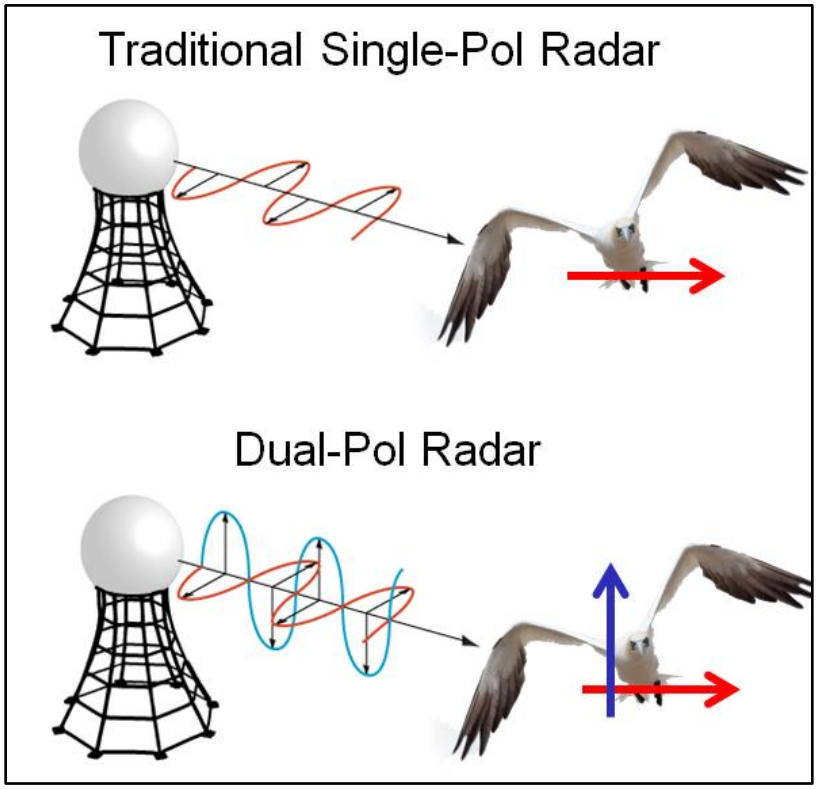

Figure 1 – Unlike traditional single polarized radar, dual-polarized radar transmits and receives power in both the horizontal and vertical polarizations. (Image modified from: http://benchmarkweb.veriskclimate.com/how-dual-pol-radar-works-better-for-hail-maps-2/)

Polarimetric products have shown great meteorological classification utility. Defined below are the standard meteorological polarimetric products and their physical representation. The utility of these metrics for bird classification will be explored later in this paper.

As a distributed target, precipitation may be described by volume reflectivity, η, which is defined as the integral sum of all scatterers contained within a pulse volume.

$$\eta = \int_0^\infty \sigma_D N_D dD \qquad [m^2/m^3] \tag{2.2}$$

Here, σ_D denotes backscatter cross section of a target, such as a water droplet, within a pulse volume containing N_D identically sized targets. We assume Rayleigh scattering conditions for dielectric spheres and back scatter cross section for each droplet with diameter D may be written as,

$$\sigma_D = \frac{\pi^5}{\lambda} |K_w|^2 D^6 \qquad [m^2] \tag{2.3}$$

K_w refers to the refractive index of water. Substituting this into the formula for volume reflectivity η yields:

$$\begin{aligned} \eta(\lambda, N_D) &= \frac{\pi^5}{\lambda} |K_w|^2 \int_0^\infty D^6 N_D dD \\ &= \frac{\pi^5}{\lambda^4} |K_w|^2 Z \qquad [m^2/m^3] \end{aligned} \tag{2.4}$$

$$Z(N_D) = \int_0^\infty D^6 N_D dD \quad [m^6/m^3] \tag{2.5}$$

Reflectivity factor is a standard meteorological metric that describes the amount of precipitation contained within the antenna's illumination volume. Reflectivity is proportional to backscatter power and is represented by the letter, $Z_{h,v}$, where h and v indicate reflectivity at either the horizontal or vertical polarization.

Differential reflectivity, Z_{dr}, measures aspect ratio and is the ratio of reflectivity at the horizontal polarization Z_h to reflectivity in the vertical polarization Z_v.

$$Z_{dr} = 10 * \log\left(\frac{Z_h}{Z_v}\right) \quad [dB] \tag{2.6}$$

Although conventional weather terminology was used throughout this thesis, it should be noted that a pulse volume in our application typically contains a single bird point-target. Here, Z_{dr} is actually used to refer to the following, more physically representative ratio:

$$Z_{dr} = 10 * \log\left(\frac{\sigma_h}{\sigma_v}\right) = 10 * \log\left(\frac{\left(\frac{64\pi^3 R^4}{G^2\lambda^2 P_t}\right)P_h}{\left(\frac{64\pi^3 R^4}{G^2\lambda^2 P_t}\right)P_v}\right) \tag{2.6}$$

$$= 10 * \log\left(\frac{P_h}{P_v}\right) \quad [dB]$$

Larger values of differential reflectivity indicate that a target is wider or more reflective along its horizontal axis.

Correlation coefficient ρ_{hv} is a measure of the similarity between both polarizations of the received echo voltages E_h and E_v:

$$\rho_{hv} = \frac{|\langle E_h E_v{}^* \rangle|}{\sqrt{\langle |E_h|^2 \rangle \langle |E_v|^2 \rangle}} \tag{2.7}$$

Values of correlation coefficient near unity suggest a target that maintains a more regular shape in time. Differential phase ψ_{dp} is the difference between H-polarized and V-polarized echo phase, and is a measure of target shape and , to some extent, water content.

$$\psi_d = \psi_h - \psi_v = \angle\langle E_h E_v{}^* \rangle \tag{2.8}$$

Differential reflectivity, correlation coefficient, and differential phase observations have been found to differ between meteorological and avian targets [2], although species based variation has yet to be fully explored.

2.2 Previous Radar Observations of Birds

Biological scatterers have been shown to have several distinct polarimetric qualities that may be exploited in a future classification algorithm. In polarimetric studies at S-band, atmospheric biota is generally associated with higher differential reflectivity than meteorological scatterers. For insects, differential reflectivity has been measured as high as 10 dB with values for birds typically between -1 and 3 dB [9].The differential reflectivity measurement corresponding to a resolution volume that contains biological scatterers often depends on the orientation of the organisms relative to the antenna boresight [4]. The correlation coefficient, which quantifies the similarity in behavior between the horizontally and vertically polarized channels in time, is often lower (0.3-0.4) for insects and birds than for meteorological scatterers (>0.8) [9]. It has been suggested that the azimuthal profile of ρhv is species dependent, but the exact variation, for the purpose of classification, has not yet been well studied [8].

Avian targets have also been observed with tracking radar to study their flight behavior [10] [11]. Here the temporal fluctuation in echo power has been used to estimate wingbeat frequency, as illustrated in Figure 2. The three different time series shown in Figure 2 represent three different types of flapping behavior, each characterized by the duration of flapping and gliding behavior. The first time series is a bird that alternates between evenly spaced flapping and gliding intervals. The second time series exhibits the

same flapping and gliding behavior, with different timing characteristics. Finally, the third time series represents a bird that flaps continuously. These variations in behavioral pattern, in addition to wing-beat frequency, correlate strongly with different species of bird [11]; this variation is explored further in this paper.

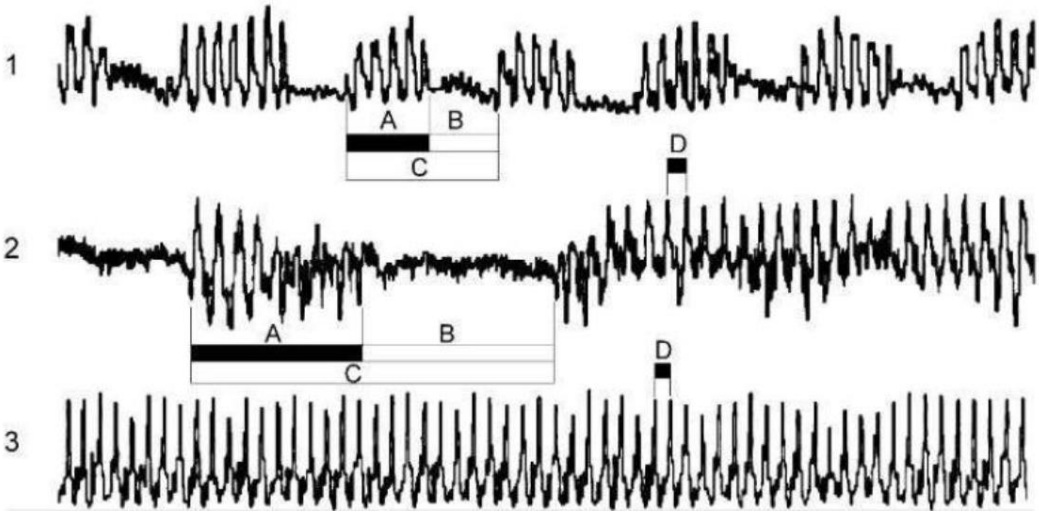

Figure 2 – Sample time-series echoes from tracking radar observations of birds with different wing-beat signatures. Gliding intervals are denoted by the interval, B, with flapping intervals labeled, A. The wingbeat period is interval, D. From [11].

The purpose of this work is to assess the metrics described above, along with new ones, for their species based classification potential. In order to do this, the UMass X-Pol weather radar was used to collect observations of migrating birds.

2.3 Hardware and Data Collection

The UMass X-Pol weather radar, shown in Figure 3, is a dual polarized X-band mobile Doppler radar originally developed measure the characteristics of weather in support of for severe storm research [12]. Based on a high-seas navigation radar with a 25 kW magnetron transmitter, it employs a 1.2m diameter parabolic dish antenna on a scanning pedestal. Doppler and polarimetric capability are achieved via coherent-on-

receive techniques, referencing the phase of the transmit pulse to the return pulse phase. System parameters are described in Table 1.

Figure 3 – Umass X-Pol weather radar

Table 1 – Umass X-Pol System Parameters

Parabolic Antenna	
Gain	41 dB
Beamwidth	1.25˚
Transmitter	
Type	Magnetron
Freq	9.41 GHz
Max Power	25 kW
Pulse Width	1 us
Duty Cycle	0.1 %
Average PRF	1 kHz
Receiver	
Gain	30 dB
Dynamic Range	60 dB
IF	60 MHz
Bandwidth	5 MHz
Noise Figure	4 dB

With a narrow antenna beamwidth (1.25º) and 41dB gain, the X-Pol radar is well suited for avian observation. The X-band radar wavelength is small, with a typical bird being larger than a single wavelength. This moves the target away from the Rayleigh scattering region, increasing the radar-cross-section. The single pulse sensitivity of the radar is shown in Figure 4, with a list of typical bird cross sections, at X-band, on the right. From the figure, it is clear that echoes from smaller birds exceed the noise floor at ranges as great as 7km. The narrow beamwidth allows the radar to discriminate among elevation angels, providing target altitude information.

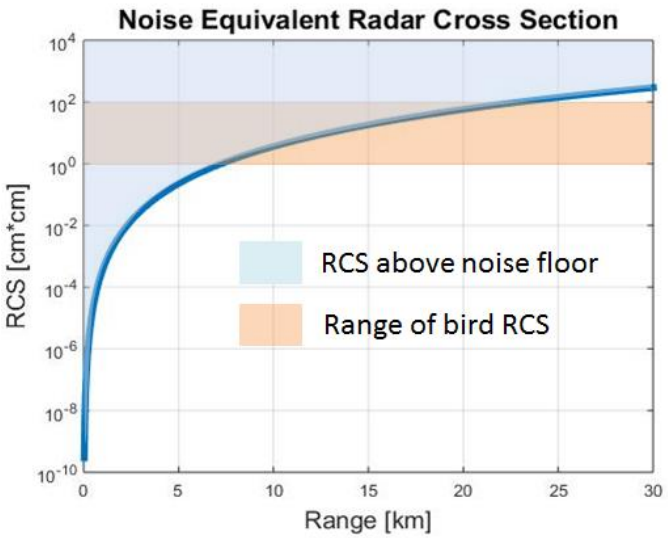

Type of Concentration	σ (cm^2)
Blackbird roosts lower Miss. Valley (winter) [127]	5–50
Single blackbird roost (winter feeding area) [112], [4]	5–50
Crows, gulls, geese, and ducks coastal areas, wildlife refuges (winter) [154]	10–500
Shearwater migration, California coast [5]	50–500
Greater Shearwater (*Puffinus gravis*) Georges Banks, non-breeding [120]	50–500
Wading and seabird (breeding) US Gulf Coast [121], [15]	50–500
Nocturnal fall migration US east of Rocky Mts. [106a]	1–50
Nocturnal fall migration, one location, eastern US [2]	1–50
Quelea (*Quelea quelea*) breeding colony, semi-arid African savannahs [38]	5–50
Quelea, semi-arid African savannahs [38]	5–50

Figure 4 – Noise-equivalent Radar Cross Section vs Range for X-Pol radar. The pink region bounds the typical cross section of most birds. Blue region represents cross sections that exceed the noise floor. The table lists common bird radar cross sections measured at X-band, from [10].

To collect study data, the radar was parked in a stationary position, looking eastward, with the antenna fixed at ten degrees elevation. The Eastward viewing angle captures birds migrating North to South. At this elevation angle, a 20 km radial range corresponds to an altitude of 3.5km. A constant pulse repetition interval of 1 kHz was

used. Time series in-phase and quadrature channel radar data was logged as birds moved through the stationary beam. Data was collected during clear air conditions in Western, Massachusetts, over ten separate evenings during Fall 2014. The full dataset contains several hundred bird observations of unknown species.

CHAPTER 3

DETECTION AND PREPROCESSING

Bird observations were a small subset of the hundreds of gigabytes of originally unfiltered dataset. In order to isolate observations of interest, a detection algorithm was used to find birds within the data and compile them into a database. Time-changing polarimetric and Doppler parameters were than extracted from each bird observation. This chapter describes the detection scheme in Section 3.1. The time-changing measurements extracted from each detection are discussed in Section 3.2, with several measured detection examples in Section 3.3.

3.1 Bird Detection Algorithm

The originally unfiltered dataset contained hours of clear-air observation, with birds flying through the beam sporadically. In order to extract the bird echoes, the data was preprocessed before applying a detection algorithm. First, data was made coherent by referencing the phase of the received echo to a copy of the transmit pulse. This is necessary due to the random nature of the magnetron based transmitter. Next, a frequency domain clutter filter was used to mitigate ground clutter returns in effected range bins. Finally, data was coherently integrated to improve signal to noise ratio. Integration parameters are captured in Table 2.

Table 2 – Parameters used for coherent integration. Time resolution of measurements will be limited by the integration period.

Integration Parameters	
Pulse Repetition Interval	1 ms
Number of Pulses Integrated	32
Integration Period	32 ms
Integration Gain	15 dB

With an integration period of 32 ms, the effective sampling rate of averaged data is 31 Hz. Wingbeat frequencies below 15.5Hz should satisfy the Nyquist criteria. From Table 3, it is clear that this frequency resolution is sufficient for all of the common birds cited in Table 3.

Table 3 - Wing-beat frequencies of several common bird species, from [13].

Taxonomic name	English name	Mass (kg)	Span (m)	Area (m^2)	Frequency ± S.D. (Hz)
Diomedea exulans	Wandering albatross	8.55	3.01	0.583	2.49±0.11
Diomedea melanophris	Black-browed albatross	3.08	2.19	0.354	2.97±0.15
Macronectes giganteus/M. halli	Giant petrel	3.24	1.98	0.326	3.14±0.19
Procellaria aequinoctialis	White-chinned petrel	1.23	1.41	0.167	3.93±0.10
Daption capensis	Cape pigeon	0.418	0.875	0.0773	5.61±0.55
Pachyptila desolata	Dove prion	0.155	0.635	0.0469	5.42±0.36
Oceanites oceanicus	Wilson's storm-petrel	0.035	0.396	0.0215	7.65±0.60
Pelecanoides georgicus	South Georgia diving petrel	0.122	0.388	0.0197	12.3±0.64
Pelecanoides urinatrix	Common diving petrel	0.133	0.408	0.0221	12.3±0.64
Phalacrocorax atriceps	Blue-eyed shag	2.23	1.13	0.183	5.85±0.25
Catharacta skua	Southern skua	1.69	1.43	0.241	3.95±0.21
Larus dominicanus	Kelp gull	0.890	1.41	0.228	3.46±0.16
Chionis alba	Sheathbill	0.610	0.822	0.105	6.35±0.29
Anas georgica	South Georgia pintail	0.437	0.682	0.0646	7.62±0.23
Cygnus cygnus	Whooper swan	8.50	2.26	0.589	3.56±0.11

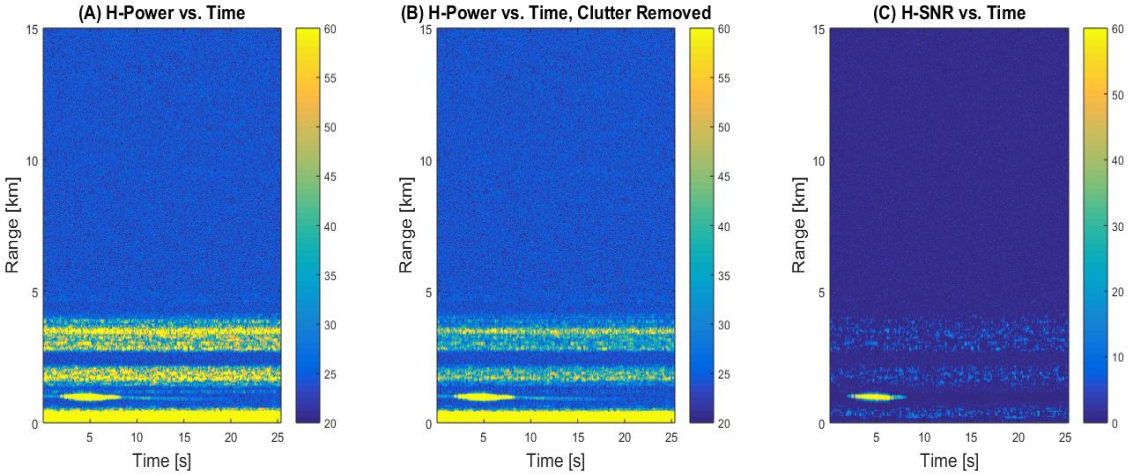

Figure 5 – (A) Coherently integrated range-time-power map. (B) Coherently integrated range-time-power map with clutter removed. (C) Range-time-SNR map of coherently integrated data with clutter removed. The bright yellow horizontal streak at 1km is a bird flying through the antenna beam.

Once detections were filtered and integrated, the range-time-power map was converted to a range-time-SNR image. Integrated data in the range-time domain, with and without clutter, along with the range-time-SNR image, is shown in Figure 5. The bright yellow horizontal streak in each Figure 5 image is a bird moving through the antenna beam. This same bird, in the range-time-SNR map, is shown in higher resolution in Figure 6A, with the corresponding time series in Figure 6B. Clearly, the detection SNR correlates well with the antenna beam shape. In order to automate the detection of birds in the data, local maxima were found within the range-time-SNR image. This was achieved by first locating all pixels in excess of a specified SNR threshold, and cataloguing them. To prevent redundant detections of a single bird, a range-time window, or "neighborhood", was specified that matched the expected duration of a bird in range and time. Pixels in excess of the SNR threshold were considered in descending order, with all detections within the same neighborhood removed from the list. A neighborhood and local maximum are shown in Figure 6A.

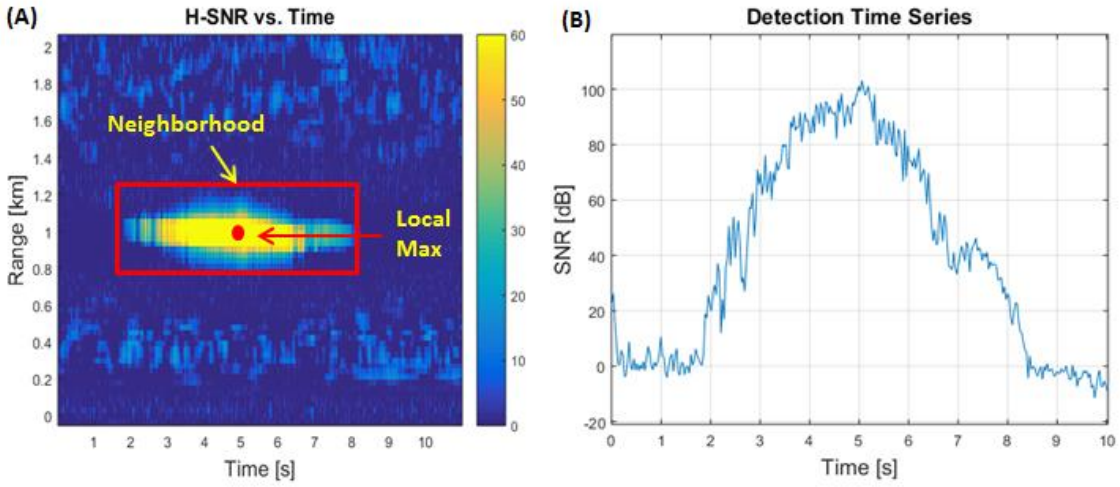

Figure 6 - (A) A bird, at 1km range, moves through the antenna beam. Neighborhood size matches the expected range and time footprint of a bird moving through the beam. (B) The corresponding SNR time series of the bird is taken from the 1km range bin.

Because bird echoes remain in the beam for an extended period of time, all pixels within the neighborhood around a local maximum were summed and compared to a second threshold. This second threshold removes short time-duration detections cause by noise. Observations exceeding the second threshold were classified as bird detections and added to the filtered data set.

3.2 Doppler Metrics

Once bird echoes were detected and extracted into a database, polarimetric and Doppler metrics were computed for each time step across the duration of the observation. These metrics change cyclically in time as the bird moves and reorients its body in flight. The following metrics were extracted for each bird according to Eq. 1 through 4, across a 32ms (32 pulse) averaging period:

1. Radar Cross Section, H-Polarization, σ_h
2. Radar Cross Section, V-Polarization, σ_v

3. Correlation Coefficient, ρ_{hv}

4. Differential Reflectivity, Z_{dr}

5. Differential Phase, ψ_{dp}

Each metric was computed across a 32ms averaging period. In addition to computing the polarimetric products, Doppler spectrum information was extracted from each bird detection. The Doppler spectrum contains information about a targets torso speed $\bar{v}$ as well as micro-Doppler signatures associated with moving parts around the torso. A spectrogram shows the way that the Doppler spectrum changes in time as a bird flaps and reorients its body. If the total received signal at the radar, for a single range bin, is given by $rx(n)$ where n is the sample index, the Doppler spectrogram $sg(w,t)$ of this signal is:

$$sg(w,t) = \left| \sum_{q=0}^{Q-1} Ham(q) * rx\big(q + (t-1)(Q-M)\big) * \mathrm{e}^{-\frac{\mathrm{j}2\pi wq}{Q}} \right|^2 \tag{3.1}$$

M is the length of overlap in the time series', of length *Q*, used to produce each subsequent spectrum, $Ham(q)$ is the Hamming window function, w denotes frequency filter bin, and *t* is the time step corresponding to each spectrum. The maximum unambiguous velocity is limited by the pulse repetition interval. At X-Band, with a 1kHz pulse repetition interval, maximum unambiguous velocity v_{max} is given by

$$v_{max} = \frac{PRF * \lambda}{4} = 7.5 \left[\frac{m}{s}\right] \tag{3.2}$$

Horizontally and vertically polarized spectrograms are shown in Figure 7. Each image column corresponds to a distinct Doppler spectrum localized in time. The bright streak moving from left to right through each image tracks the torso speed of the bird in

time. Spectral width introduced around the torso track represents return power from moving parts on the bird during flapping behavior. During intervals of increased spectrum width (i.e. flapping), the bird in Figure 7 exhibits torso speed changes. Physically speaking, this change in speed is a result of the flapping behavior. For a bird that is flying perpendicular to the radar, this change in speed would not be observed. Spectrograms vary greatly between birds; two additional examples are shown in Figure 8 and Figure 9 respectively.

It should be noted that detection signal-to-noise ratio for the vertically polarized channel is consistently lower than the horizontal polarization. For birds with greater body width than height, this tendency makes sense. As discussed earlier, differential reflectivity for volumetric avian targets at S-band has typically been measured between -1 and 3 dB, although values as high as 10dB have been observed [9]. However, it is possible that the radar was not perfectly calibrated. Fortunately, the feature extraction method presented in this thesis generally does not rely on absolute measurement values. Instead, meaningful features describe the way that measurements change in time with respect to themselves and each other as the bird cycles through different behavioral states (i.e. flapping and gliding).

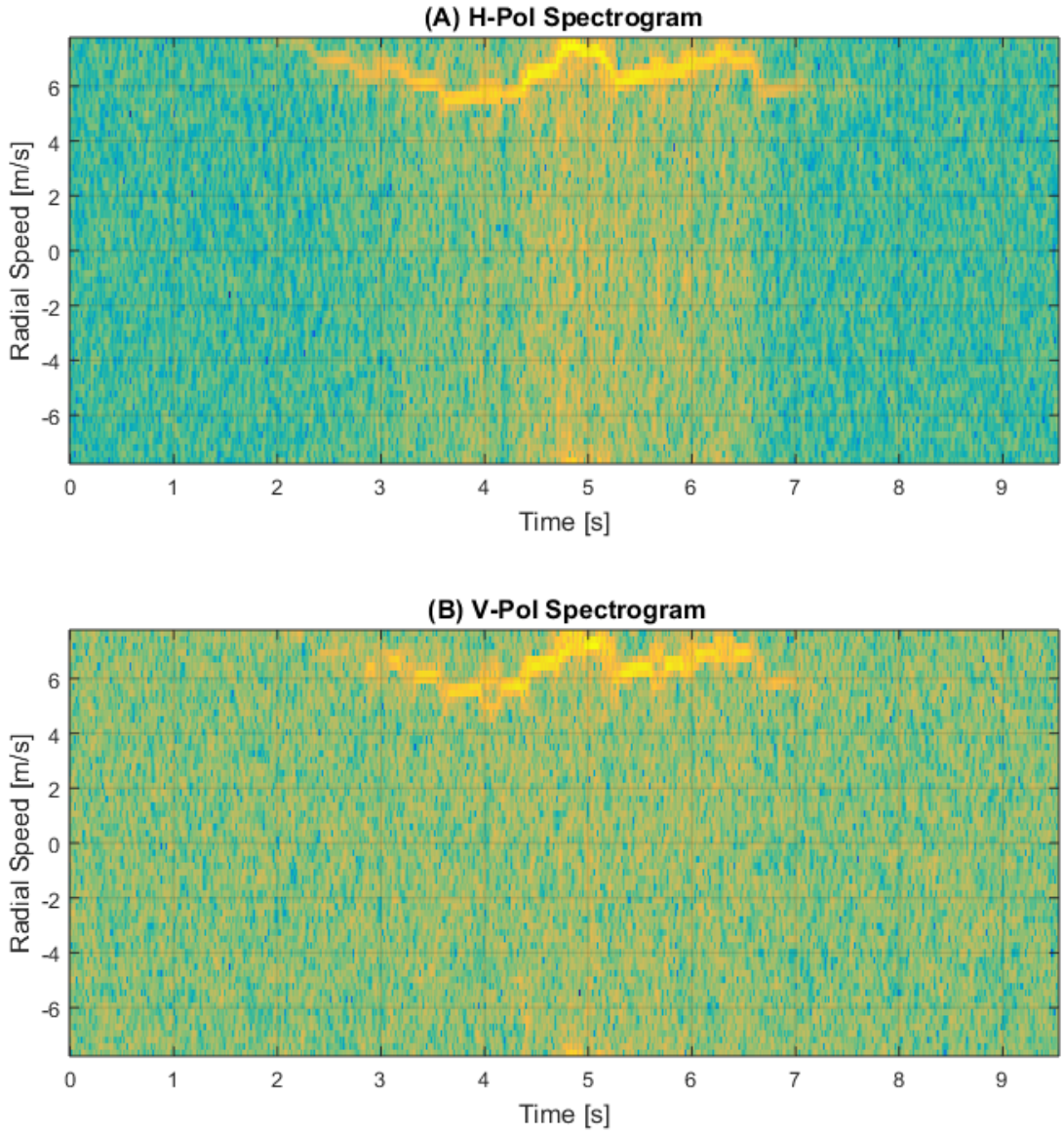

Figure 7 – Horizontally (A) and vertically (B) polarized spectrograms show the Doppler spectrum as it changes in time. The torso speed is tracked by the bright streak moving left to right through time. Regions with greater spectral spreading around the torso indicate echo power returning from moving parts of the bird during flapping behavior.

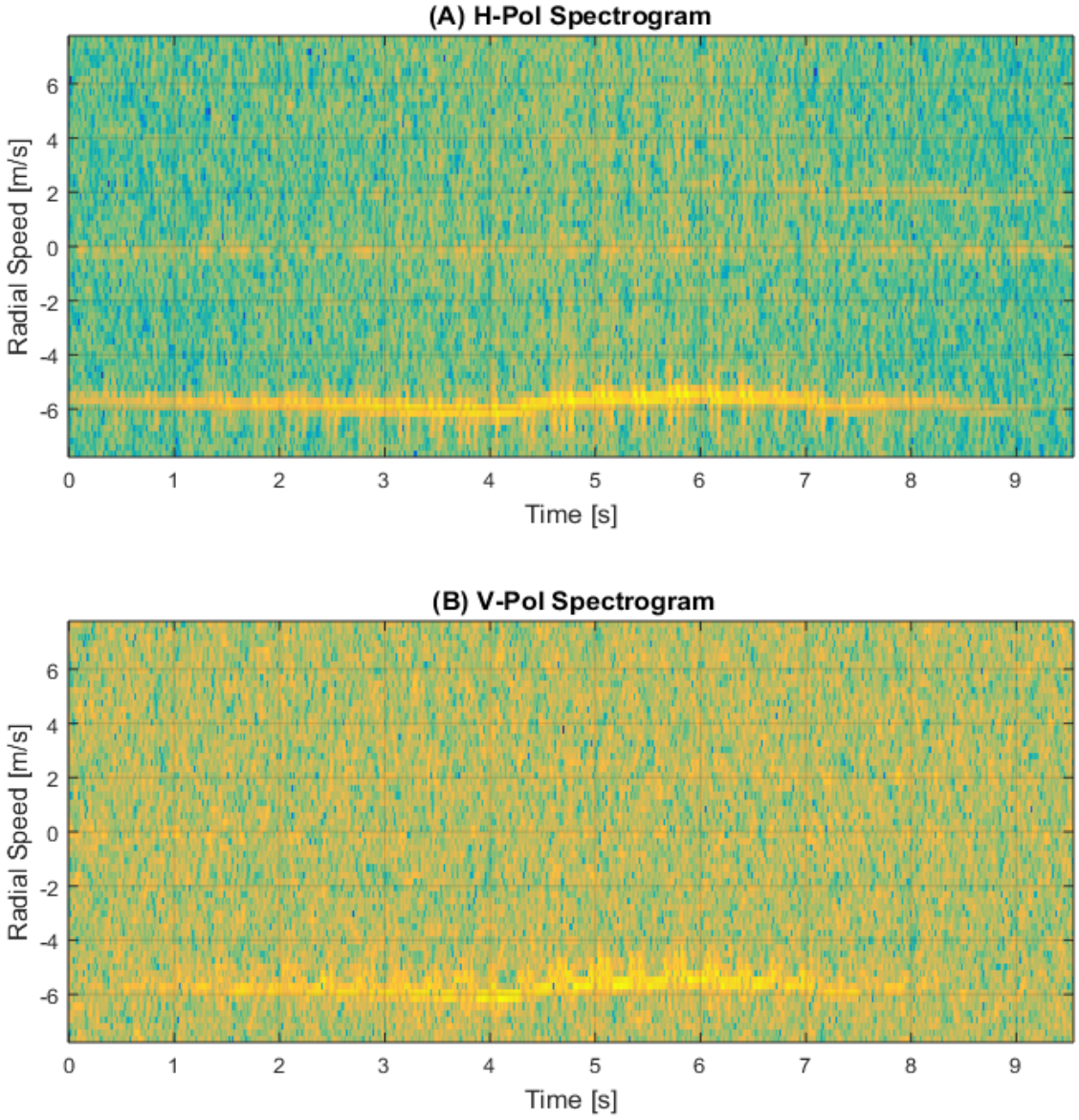

Figure 8 - Horizontally (A) and vertically (B) polarized spectrograms show the Doppler spectrum as it changes in time. The torso speed is tracked by the bright streak moving left to right through time. Regions with greater spectral spreading around the torso indicate echo power returning from moving parts of the bird during flapping behavior. This bird alternates between periods of flapping and gliding. Flapping intervals have a different appearance in the H and V polarizations.

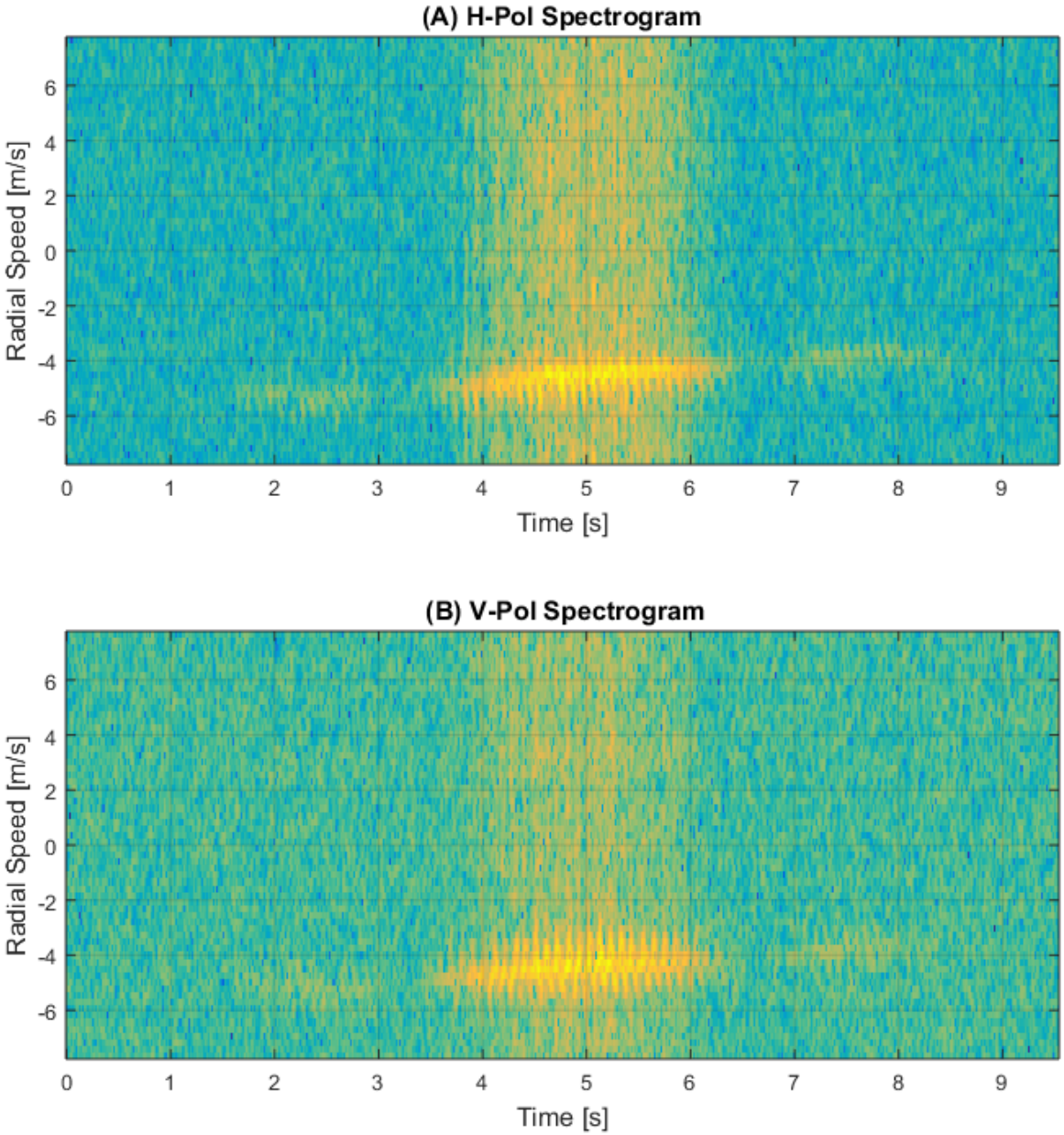

Figure 9 - Horizontally (A) and vertically (B) polarized spectrograms show the Doppler spectrum as it changes in time. The torso speed is tracked by the bright streak moving left to right through time. Regions with greater spectral spreading around the torso indicate echo power returning from moving parts of the bird during flapping behavior. This bird continuously flaps at a constant frequency.

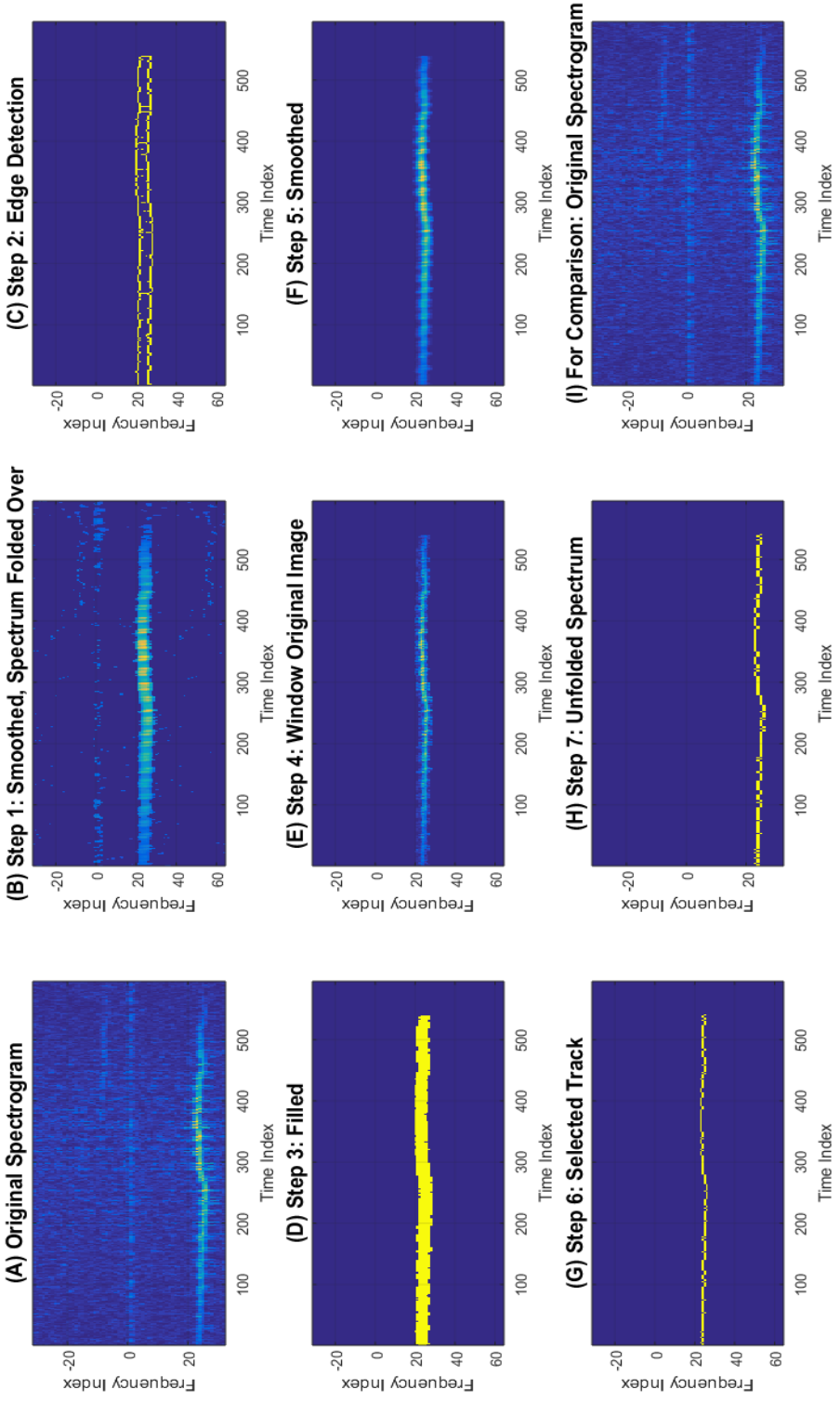

Figure 10 - (A) through (G) show intermediate steps in the torso velocity extraction algorithm, with the result in (H)

Micro-Doppler features are isolated by normalizing the bird's torso velocity to the zero-velocity frequency bin the spectrogram image. In order to do this, the torso speed must first be extracted from the image for each time step. Because the brightest bin in each spectrum does not always correspond to the torso speed, a more complete approach was used to determine the torso speed at each time. The steps involved are listed below, with the output of each stage displayed in Figure 10.

1. The top half (i.e. all positive radial velocities) of the original spectrogram, shown in Figure 10 (A), is appended to the bottom of the original spectrogram[1]. The image is smoothed with a moving average filter[2] and the lowest eighty five percent of pixels are zeroed. The resulting image is shown in Figure 10 (B).
2. The Canny edge detection algorithm [14] is applied to the image, as shown in Figure 10 (C).
3. Next, morphological operations are applied[3], first dilation and then erosion, to fill regions enclosed by the edge detections (Figure 10 (D)). The largest filled region ('blob') is maintained, while all others are zeroed.
4. All pixels in the original spectrogram that overlap with the yellow region in Figure 10 (D) are multiplied by unity, all other pixels are zeroed (Figure 10 (E))

[1] This step serves to create a continuous torso velocity track through the image in cases where aliasing has occurred *and* the torso velocity track crosses the maximum unambiguous velocity. In these cases, a portion of the torso velocity track may be in the top half of the image, with the other half on the bottom.

[2] The averaging window is five frequency bins high and three spectrums wide.

[3] Morphological operations use a 9x9 pixel, diamond-shaped , structuring element.

5. A moving average filter[4] is applied to (E) to smooth the image, resulting in Figure 10 (F).
6. The brightest pixel in Figure 10 (F) is selected for each spectral column and classified as the pixel corresponding to the torso velocity (Figure 10 (G).
7. Finally, the bottom third of the image (the copied half of the original spectrogram) is cropped and added to the middle third (i.e. negative velocity region) of the image, resulting in Figure 10 (H).

Selecting the torso track from within a 'blob' region provides added robustness in scenarios with strong clutter or noise. For example, the data shown in Figure 10 contains some ground clutter that does not impact the selected torso velocity track in any way.

Because standard bird flight speeds are known to exceed the maximum unambiguous velocity of the X-Pol radar system, the torso velocity may need to be unfolded. For this reason, the original range-time-power image is evaluated for migration in range. Figure 11 shows a bird detection in the range-time-power domain. Here the bird echo appears closer to the radar at later times, as indicated by the dashed red line. In this case, the radial velocity is determined to be negative and the torso velocity vector is unfolded if necessary. In order to automatically determine if a given bird is moving towards or away from the radar, a line is fit through the detection as shown in Figure 11. The slope of this line, along with the tightness of the fit, are used to determine if the bird is clearly moving towards or away from the radar. Birds that have no clear radial direction are assumed to have an un-aliased torso velocity.

[4] The averaging window is three frequency bins high and three spectrums wide.

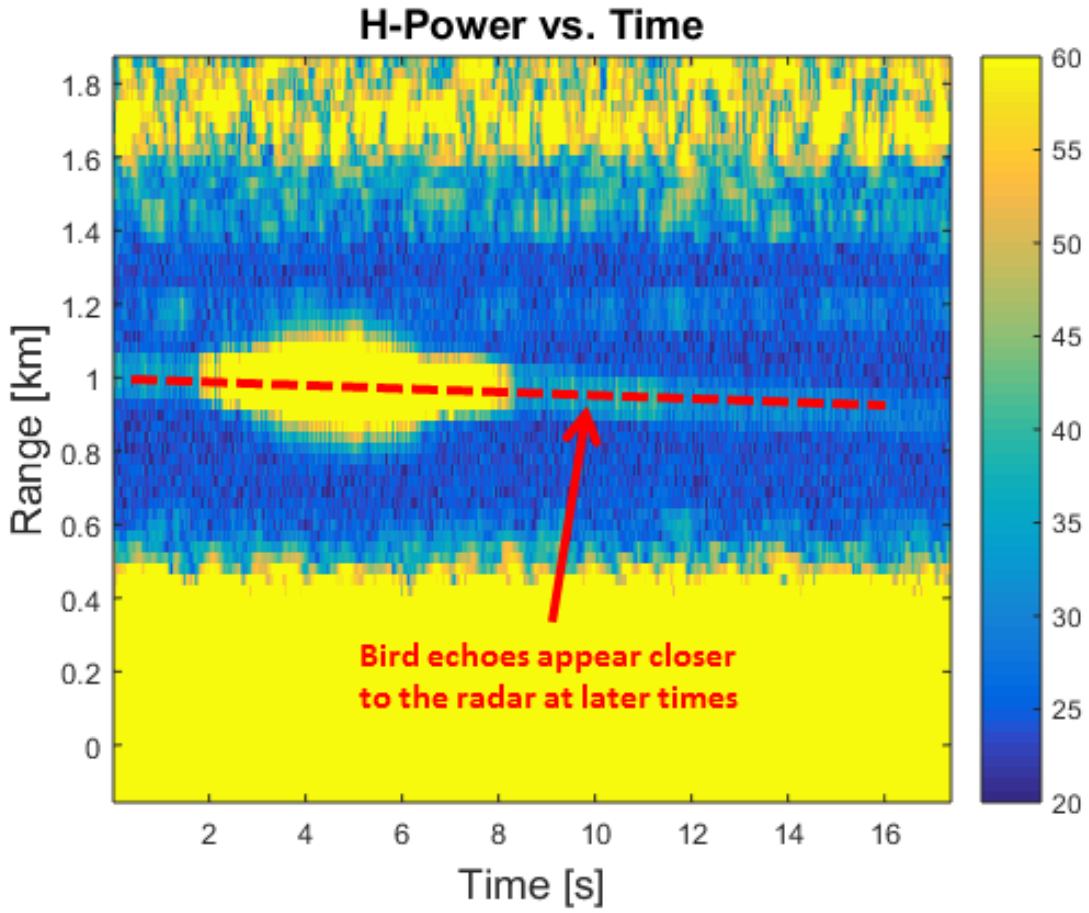

Figure 11 – Here, bird echoes appear closer to the radar at later times. The range-time-power map may indicate the direction of flight when the Doppler velocity is ambiguous.

Once the torso velocity has been extracted, and unfolded if necessary, the original spectrogram may be normalized to isolate the micro-Doppler signatures. Normalization is achieved by circularly shifting each spectrum so that the torso velocity is centered in the spectrogram. Figure 12 shows the original spectrogram (A), the extracted torso velocity (B), and the normalized spectrogram (C). Meaningful micro-Doppler signatures are primarily contained in the rows of the image closest to the torso speed, so the radial speed axis is cropped. Finally, Doppler spectrum widths, σ_h and σ_v, are calculated for each polarization, at each time step.

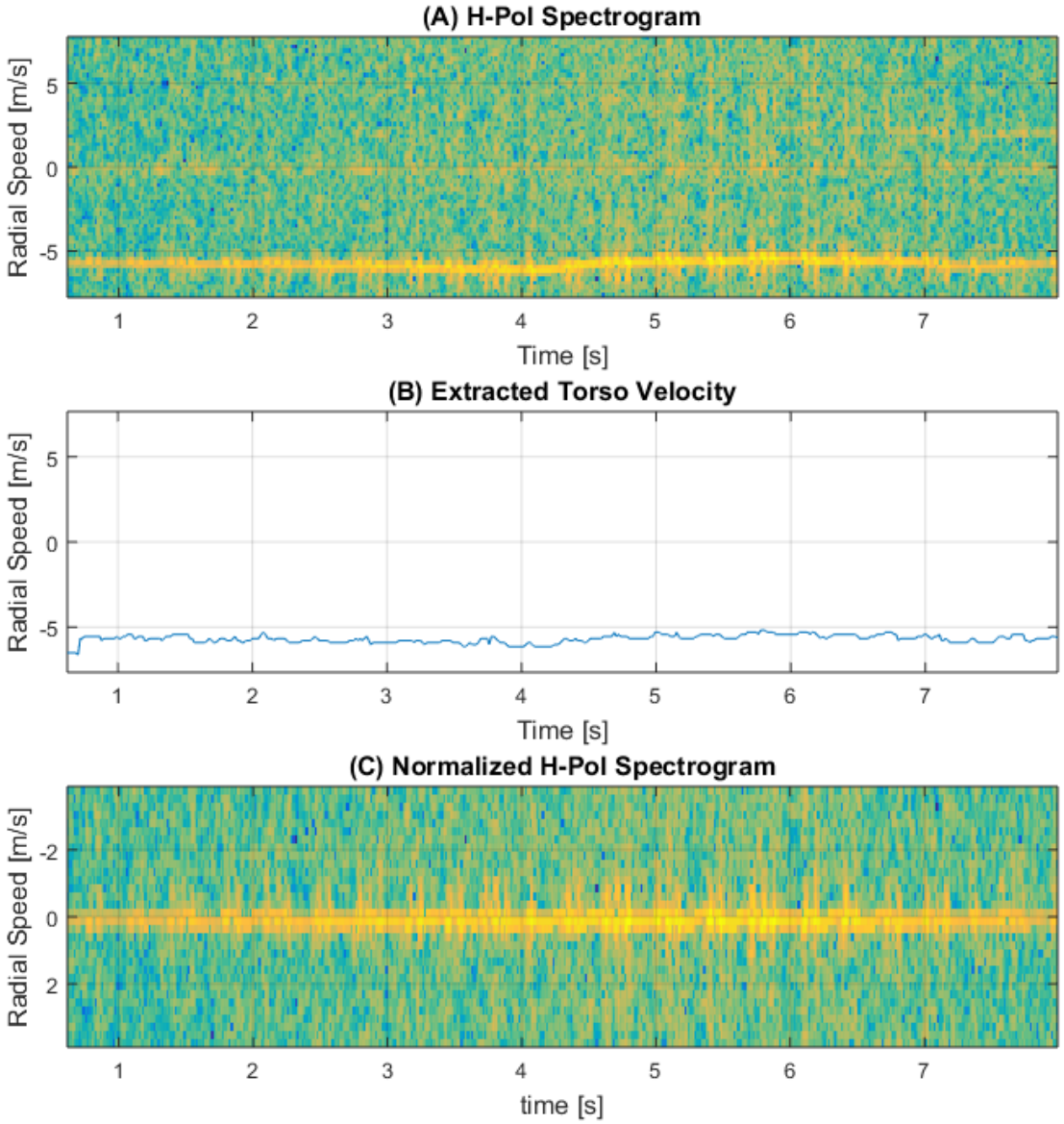

Figure 12 – Torso velocity (B) is extracted from the original spectrogram (A), and used to produce the normalized spectrogram (C). The radial speed axis of the normalized spectrogram is cropped to highlight the micro-Doppler signatures.

3.3 Sample Observation Time-Series

As a bird moves through the antenna beam, its time changing behavior may be recorded in terms of the Doppler and polarimetric measurements described above.

Measurements were found to fluctuate significantly as the body orientation, shape, and speed change. The way that these measurements change in time varied between Bird detections. Figure 13, Figure 14, and Figure 15 include three different bird observations, with corresponding polarimetric and Doppler measurements in time. These three examples illustrate three different types of temporal behavior in flight and matching measurement fluctuations.

The bird shown in Figure 13 exhibits evenly spaced intervals of flapping and gliding. In horizontally and vertically polarized spectrograms, Figure 13(A) and Figure 13(B) respectively, flapping intervals are characterized by increased spectrum width about the torso speed. Spectrum width indicates echo power returning from parts of the bird that are moving with respect to the torso. Wider spectrum width represents greater relative speeds, while brighter pixels suggest more reflective, sometimes larger, moving parts.

Periods of flapping are also marked by lower echo power in both polarizations, Figure 13(C) and Figure 13(D), although this difference is larger in the horizontal polarization than in the vertical polarization. Physically speaking, this means that this particular bird appears 'bigger' to the radar when its body assumes a gliding position, although this is not universally the case for all birds and orientations.

For a well calibrated system, higher differential reflectivity suggests a target that is more reflective, or potentially longer, in the horizontal polarization. For a bird, this may physically occur when its wings are outstretched during gliding periods, as measured in Figure 13(E). Higher values of correlation coefficient

indicate a fairly constant aspect-ratio in time. When a bird holds its body in a fixed gliding position, this is likely to occur, and higher values are measured, as shown in Figure 13(F). Finally, all measurements, including torso speed and differential phase, Figure 13(G) and Figure 13(H), generally appear more variable during flapping intervals, matching the dynamic nature of this behavioral state.

Although correlation coefficient was generally found to be higher during gliding periods for all birds, the other measurements tend to vary differently by bird; Figure 14 and Figure 15 show two alternative examples. The bird in Figure 14 alternates between periods of flapping and gliding in a way that is less periodic than the bird in Figure 13. Another key difference is that the bird in Figure 14 appears much 'brighter' to the radar in the vertical polarization when it is in certain stages of its flapping cycle, rather than during gliding behavior. As previously mentioned, this tends to vary by bird observation, and is likely a function of orientation and species. Lastly, unlike the previous two examples, the bird in Figure 15 flaps continuously at a constant rate. As it flaps, it cycles its body through a finite set of positions and the measurements change accordingly with the same periodicity.

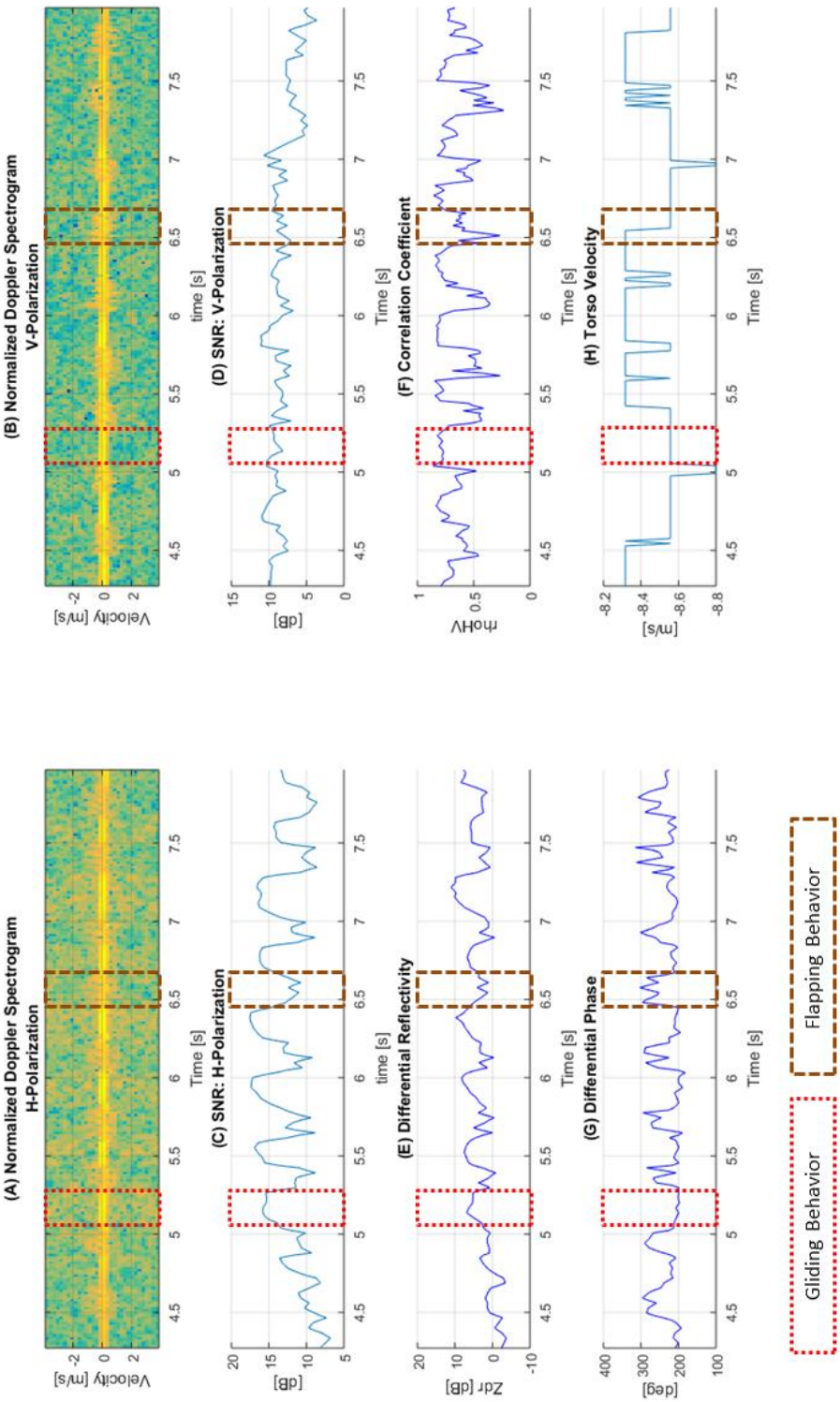

Figure 13 –Time series measurements for a bird alternating between evenly spaced flapping and gliding intervals. (A) Horizontally-polarized spectrogram, (B) vertically-polarized spectrogram, (C) h-polarized signal-to-noise ratio, (D) v-polarized signal-to-noise ratio, (E) differential reflectivity, (F) correlation coefficient, (G) differential phase, and (H) torso velocity in meters per second.

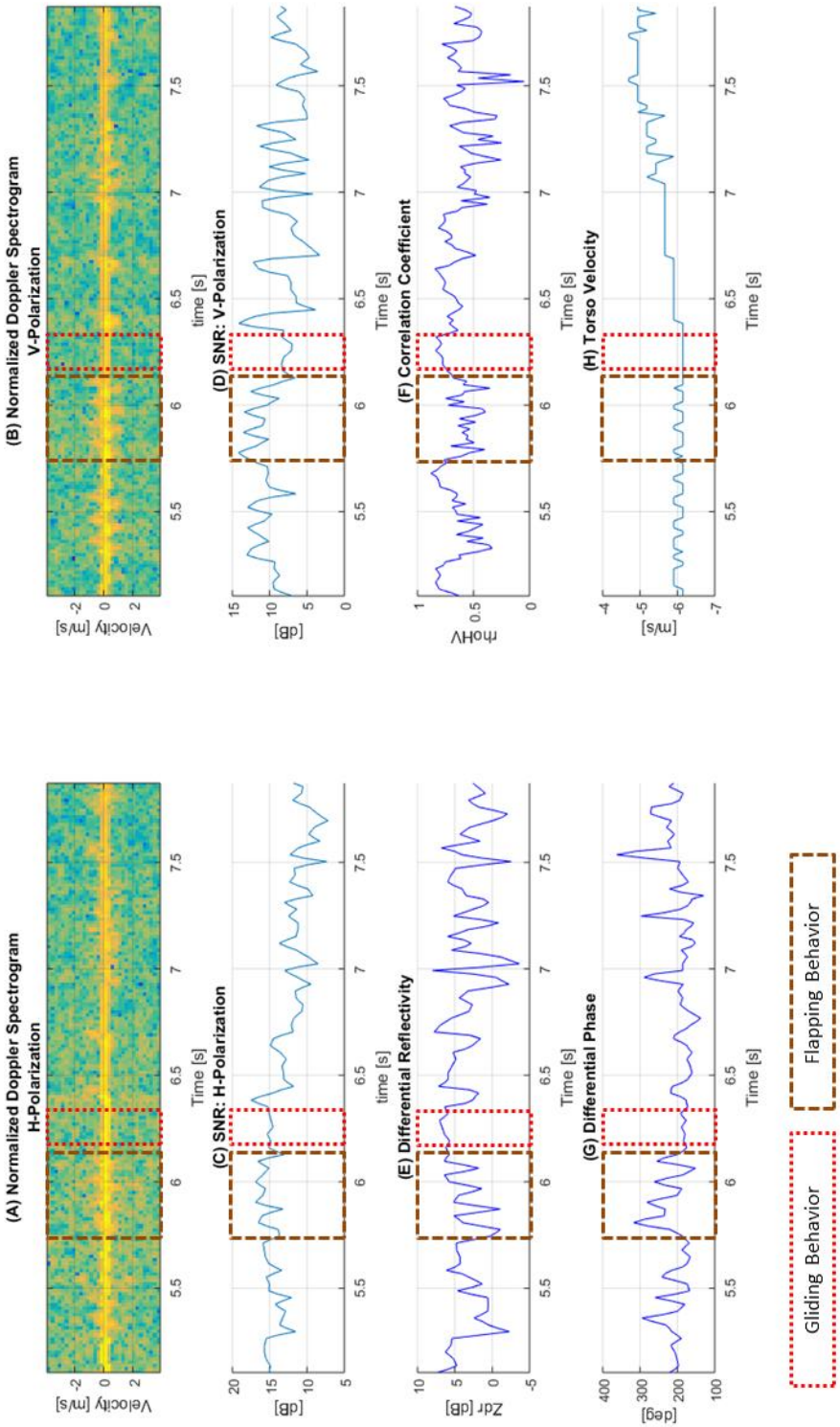

Figure 14 - Time series measurements for a bird alternating between sporadically spaced flapping and gliding intervals. (A) Horizontally-polarized spectrogram, (B) vertically-polarized spectrogram, (C) h-polarized signal-to-noise ratio, (D) v-polarized signal-to-noise ratio, (E) differential reflectivity, (F) correlation coefficient, (G) differential phase, and (H) torso velocity in meters per second.

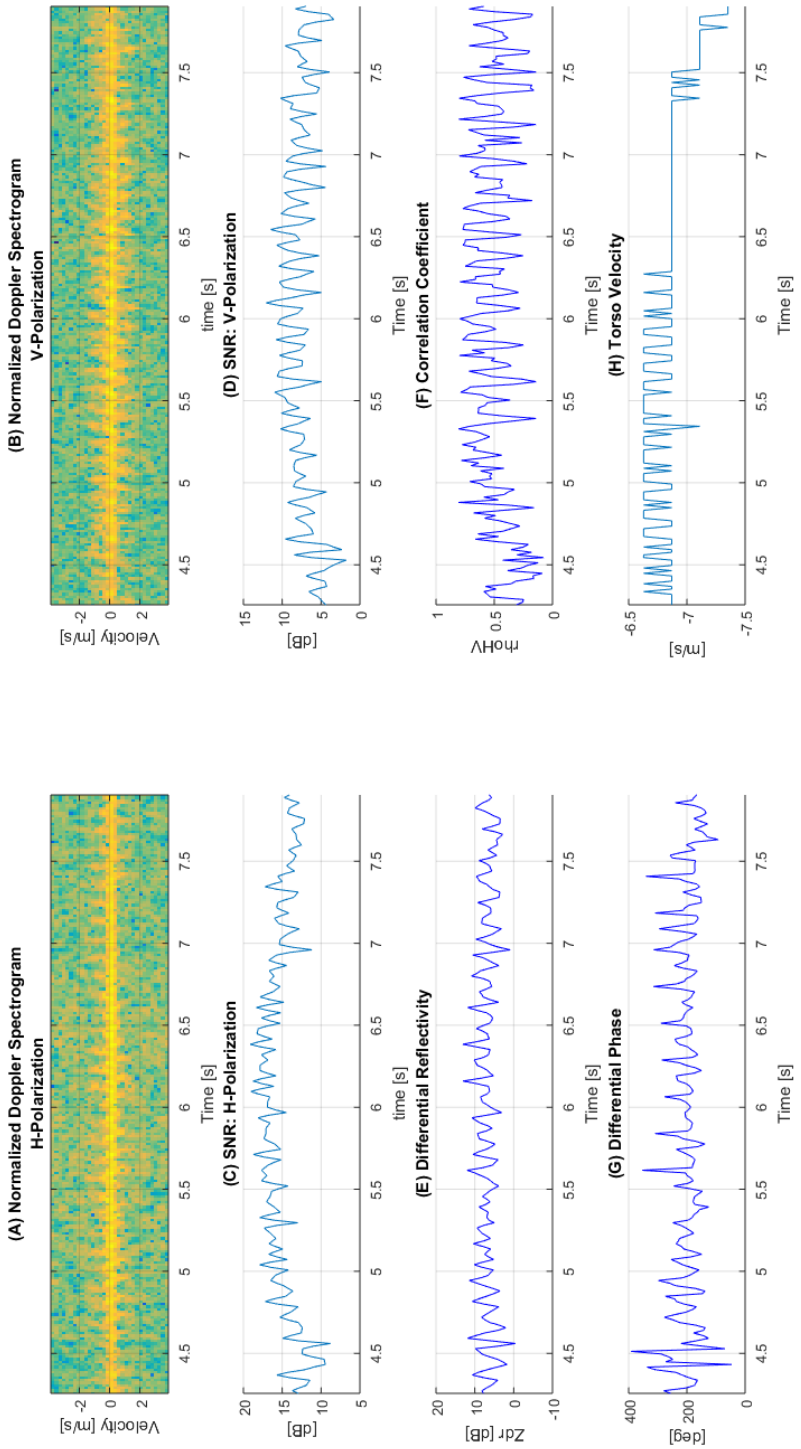

Figure 15 - Time series measurements for a bird flapping at a constant rate. (A) Horizontally-polarized spectrogram, (B) vertically-polarized spectrogram, (C) h-polarized signal-to-noise ratio, (D) v-polarized signal-to-noise ratio, (E) differential reflectivity, (F) correlation coefficient, (G) differential phase, and (H) torso velocity in meters per second.

CHAPTER 4

FEATURE EXTRACTION

The stated objective of this thesis is to analyze radar echoes from birds for species based variation. Because truth data was un-available, the goal was *not* to tie variation to specific species. This level of analysis will require a more extensive dataset. In order to provide a meaningful comparison between bird observations, a feature vector, derived from the time-changing radar measurements, must be produced for each bird. The challenge of producing a meaningful feature vector is summarizing time-changing radar measurements into meaningful time-independent metrics. As shown in Chapter 3, measurement fluctuations in time are physically meaningful, and not random. For this reason, simply averaging a time-series measurement across all time stamps results in a loss of meaningful temporal and statistical information, and provides an incomplete description of the target.

Based upon the observation that time-changing radar signatures may be mapped to meaningful behavioral states (i.e. flapping and gliding), an alternative feature extraction approach was designed. This approach has two stages, as illustrated in Figure 16. During the first stage, each time-step across a single detection is assigned a *behavioral state*. The time changing radar measurements, '*Feature Space One'*, are used to make this assignment. The algorithm designed to perform this step is described in Section 4.1.

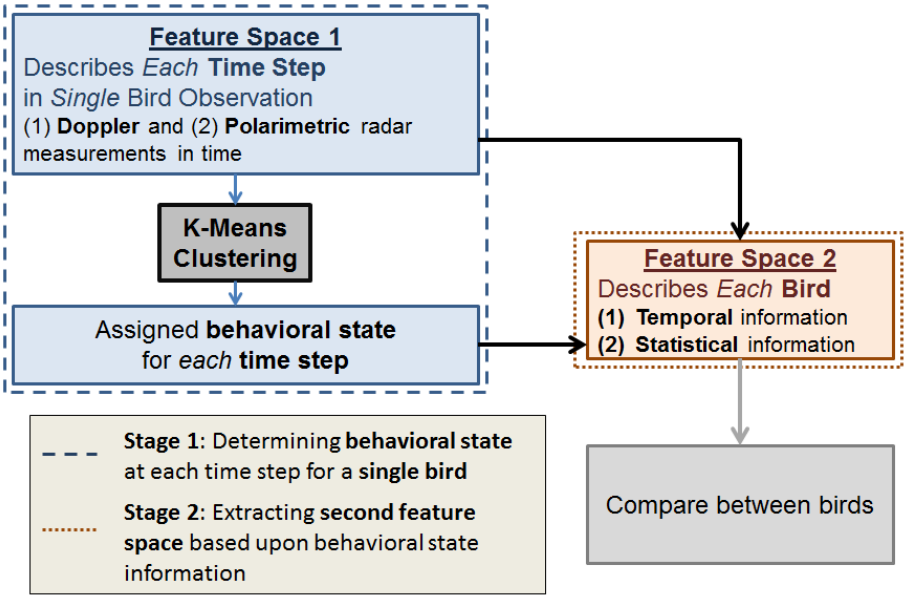

Figure 16 - A two stage feature extraction approach is used to provide a meaningful description of a given bird. Stage one involves mapping each time stamp across the duration of a bird observation to one behavioral state, based upon the radar measurements at that time. The second feature extraction stage produces a second set of features derived from the assigned behavioral state. These include (1) temporal features which describe the frequency and order of a birds different behavioral states and (2) statistical features which summarize the typical values of radar measurements during each behavioral state

Once the behavioral state of a bird is known at each point in time, a second layer of physically meaningful information, '*Feature Space Two'*, may be extracted from each bird detection. This process is outlined in Section 4.2. Feature Space 2 includes (1) temporal and (2) statistical features. *Temporal* features describe the way that a bird cycles through different behavioral states in time[5]. *Statistical* features describe the way that a bird looks to the radar while in each behavioral state, in terms of the original time changing radar measurements. For example, Figure 13 and Figure 14 showed that correlation coefficient is higher during gliding intervals. Exactly how much higher is a function of species and orientation. When the behavioral state of a bird is known at each

[5] Ecologists have long known that temporal flight behavior varies by species [8].

point in time, we are in a position to go back and compute the average correlation coefficient across all gliding intervals.

4.1 Feature Extraction Stage One: Assigning Behavioral State

The first stage of the two step feature extraction approach involves mapping each time step across a single bird observation to one of a predefined set of behavioral states. As shown in Chapter 3, Figure 13, Figure 14 and Figure 15, radar measurements change in time with the changing behavioral state of a bird. In essence, flapping and gliding behavioral states look different in terms of the radar measurements.

The k-means clustering algorithm was used to sort all time-stamps into different behavioral groups. K-means takes, as inputs, a list of 'observations', $(\boldsymbol{x}_1, \boldsymbol{x}_2, \dots, \boldsymbol{x}_n)$, where each observation is defined as a 'feature vector' of length m. These observations are then sorted into a pre-specified k-number of 'output clusters', $\boldsymbol{C} = \{C_1, C_2, \dots, C_k\}$, based upon the values contained in the feature vectors. Observations are assigned to clusters so as to minimize the total distance of all observations within a given cluster from its centroid. If $\boldsymbol{\mu}_i$ is an m-length vector denoting the centroid of all observations in cluster C_i, the optimal cluster assignment satisfies:

$$\underset{\boldsymbol{C}}{\operatorname{argmin}} \sum_{i=1}^{k} \sum_{x \epsilon C_i} \|\boldsymbol{x} - \boldsymbol{\mu}_i\|^2 \tag{4.1}$$

In our application, each observation is a time step, during a single bird detection, with n total time stamps across the entire detection. The corresponding feature vector, *Feature Space One*, contains radar measurements at that time; a complete set of these features will be described in more detail in Section 4.1.1. In our case, $k = 3$ output

clusters represent three possible behavioral states: one gliding state and two flapping states. The reason for three states, as opposed to two, will be further discussed in the next section. Sample behavioral clustering results will be shown in Section 4.1.2, with a ranking of feature utility in Section 4.1.3. Finally, Section 4.1.4 will explain why this novel method is far superior to conventional techniques for extracting temporal information, like wing-beat frequency.

4.1.1 The First Feature Space

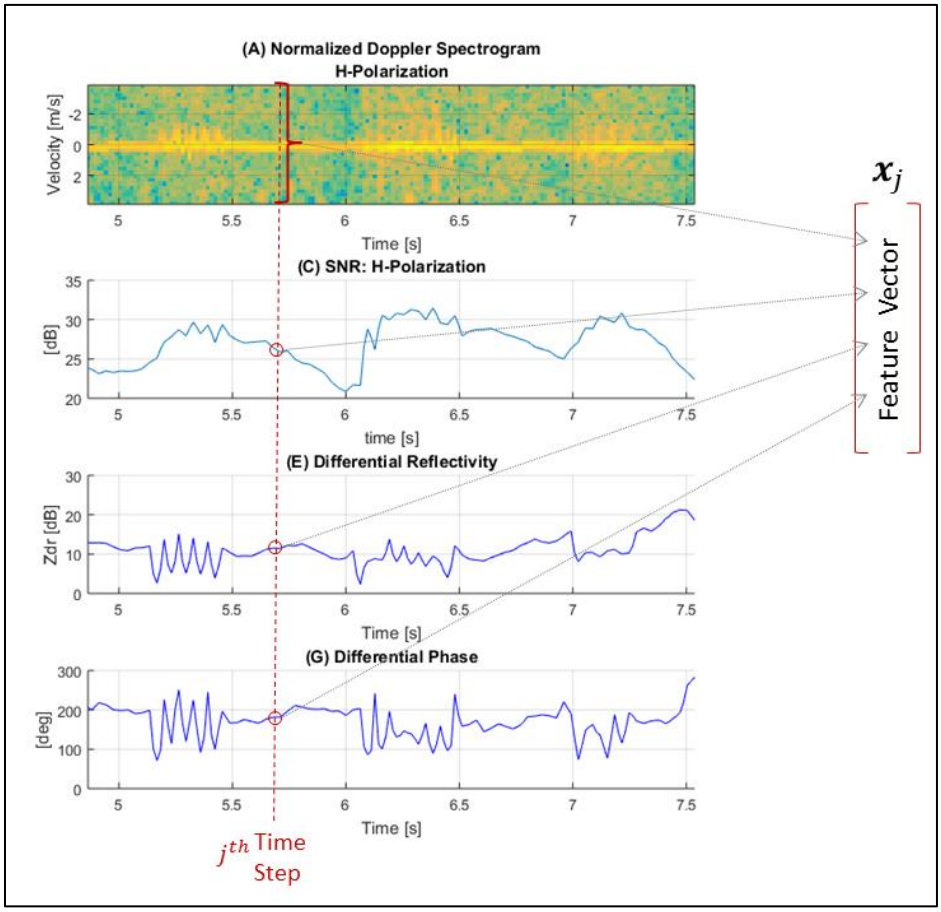

Figure 17 – The feature vector for the jth time stamp contains radar measurements from that time. These measurements include, but are not limited to, ten central pixels from each spectrogram, horizontal and vertical power, differential reflectivity, and differential phase.

As mentioned previously, the k-means clustering algorithm is applied to all time steps, assigning each to one of three possible behavioral states (clusters). As shown in Figure 17, a feature vector may be produced for each time step, containing radar measurements from that time. Nine central pixels of the spectrogram, representing speeds closest to the torso velocity, are included as features in order to capture spectral information associated with flapping behavior. As depicted in Figure 17, horizontally polarized signal-to-noise ratio, differential reflectivity, and differential phase may also be used as features. A comprehensive list of features is included in Table 4.

Table 4 – List of features used for behavioral clustering

	Feature
1	Horizontally-polarized power[6]
2	Vertically-polarized power
3	Correlation coefficient
4	Differential phase
5	Differential reflectivity
6	Horizontally-polarized spectral width
7	Vertically-polarized spectral width
8	Differential-spectrum width
9	Horizontally-polarized Doppler spectrogram row at $\bar{v} \mp n\Delta v$, for integer n where $\lvert n \rvert \leq 4$
10	Vertically-polarized Doppler spectrogram row at $\bar{v} \mp n\Delta v$, for integer n where $\lvert n \rvert \leq 4$

Key:

$\bar{v}$ is the torso speed, normalized to the center of the spectrogram. Δv denotes the width of each Doppler bin in [cm/s].

"H-Polarization at $\bar{v} + n\Delta v$" represents a row of the H-Polarized spectrogram, offset from the venter by n Doppler bins.

[6] Because this clustering procedure is solely focused *on time-variation* of measurements, converting power to radar cross section or reflectivity is unnecessary. In other words, we are comparing measurements at time steps within a single detection to each other. Further normalization occurs later to provide desired spread and weighting.

In addition to the features listed in Table 4, the feature vector for each time stamp also included (A) the first derivative of each of these measurements as well as (B) all measurements and derivatives at four adjacent time steps (two on each side).

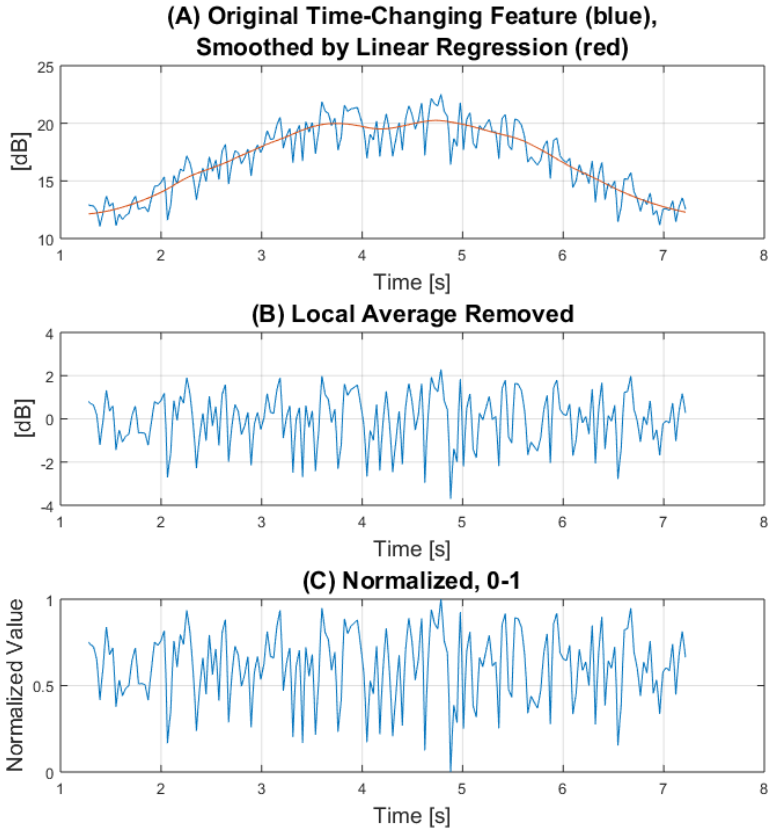

Figure 18 – Prior to implementing the k-means clustering algorithm, features are normalized and scaled.

Before applying the k-means clustering algorithm, each feature was smoothed using local linear regression to determine local effects of the antenna pattern and normalized accordingly. The purpose of this step is to remove the local average, isolating the meaningful variation and enabling equal comparison between all time steps. Figure 18(A) shows the original feature, z, in blue with the smoothed copy in red z_{smooth}. The red line represents the changing gain as the bird moves through the antenna beam. Subtracting this bias,

$$y_{norm} = y - y_{smooth} \tag{4.2}$$

removes the dominant[7] effects of underlying system gain, resulting in y_{norm} as shown in Figure 18(B). Finally, features are rescaled before applying weighting (W):

$$y'_{norm} = W * \left(\frac{y_{norm} - \min(y_{norm})}{\max(y_{norm}) - \min(y_{norm})} \right) \tag{4.3}$$

A sample y'_{norm} is shown in Figure 18(C).

4.1.2 Determining Instantaneous Behavioral State

Once the features have been selected and prepared , k-means clustering is applied with $k = 3$ behavioral states. These behavioral states are defined as follows:

State 1	**Gliding**
State 2	**Flapping**: Type 1
State 3	**Flapping**: Type 2

Two states were selected to describe flapping behavior in order to convey temporal information during flapping intervals (i.e. wingbeat frequency). Sample clustering results, for the same birds as in Figure 13, Figure 14, and Figure 15, are shown in Figure 19, Figure 20, and Figure 21 respectively, along with some of the original measurements for reference.

[7] Further adjustments were explored to addressing residual effects of antenna pattern but were found to offer minimal performance improvement. Certainly with more time, this should be revisited.

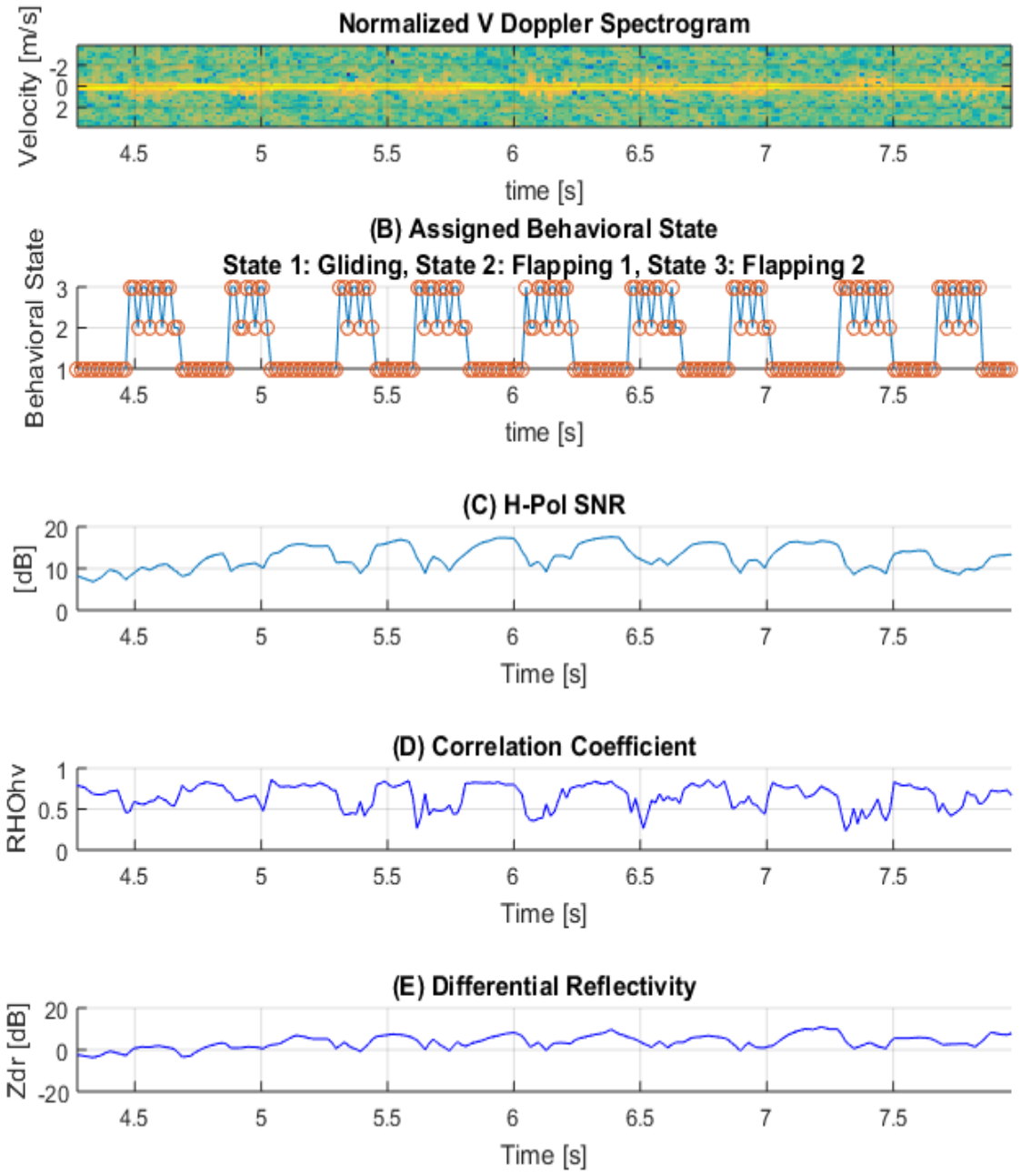

Figure 19 - This bird, the same as in Figure 13, alternates between flapping and gliding behavior in evenly spaced intervals. (B) Behavioral clustering results indicate that this information has been successfully captured. (A)(C)(D) and (E) contain time series measurements for reference.

As described in Chapter 3, the bird depicted in Figure 19 alternates between evenly spaced flapping and gliding intervals. It is clear from Figure 19 (B) that this

temporal information has been captured in the behavioral clustering results. Here, red dots indicate the assigned state at each time step. State 1, gliding, persists for extended intervals. During flapping behavior, the bird oscillates between Flapping: Type 1, and Flapping, Type 2, capturing the temporal information of its flapping cycle. From Figure 19 (C), it seems that gliding intervals might have been isolated using correlation coefficient alone. However, wing-beat information during flapping intervals would not have been so easily extracted using conventional Fourier transform based methods on any of the time series shown in Figure 19. The behavioral state output from the clustering procedure produces clean and localized temporal information about this bird's flight behavior. As previously discussed, this type of temporal information is one of the best established mechanisms for distinguishing between birds of different species.

Figure 20 (B) shows the results of behavioral clustering for a different bird. As previously discussed in Chapter 3 (Figure 14), this bird alternates between flapping and gliding in a way that is less periodic. This bird has extended gliding intervals that are successfully identified, however, unlike the bird discussed in Figure 19, this bird cycles through all three behavioral states during flapping intervals. Physically, this may be due to a portion of the flapping cycle that involves similar body mechanics to gliding. For this reason, this result is also meaningful. However, when these clustering results are used to compute a second set of features (Sections 4.2), care is taken to ensure that temporal features extracted from assigned behavioral states are comparable between *all* bird detections. Finally, like the bird in Figure 19, the localized temporal information contained in these results would be difficult to obtain using conventional methods.

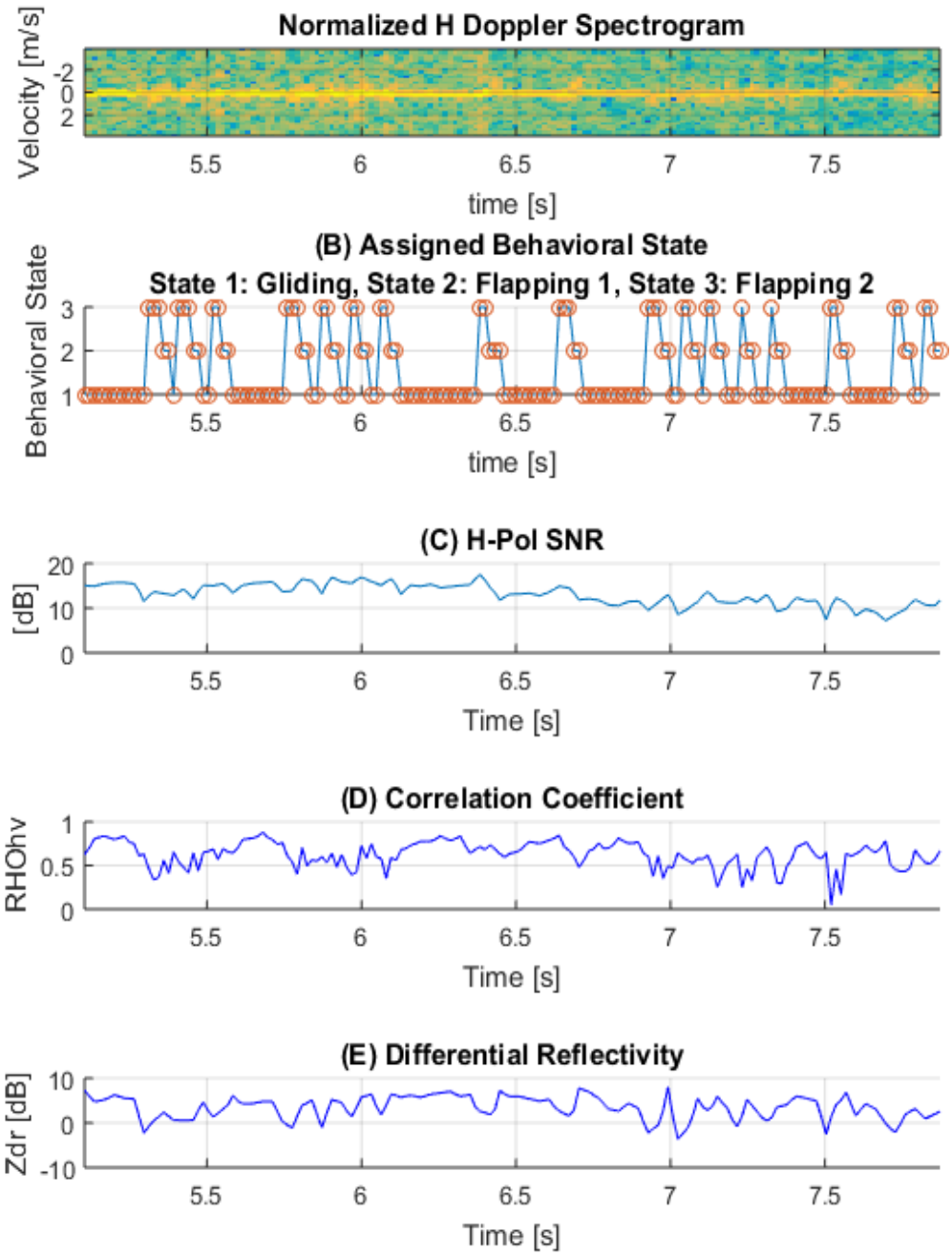

Figure 20 - This bird, the same as shown in Figure 14, alternates between flapping and gliding behaviors in a non-periodic way. (B) Assigned behavioral states capture this temporal information. (A)(C)(D) and (E) contain time series measurements for reference.

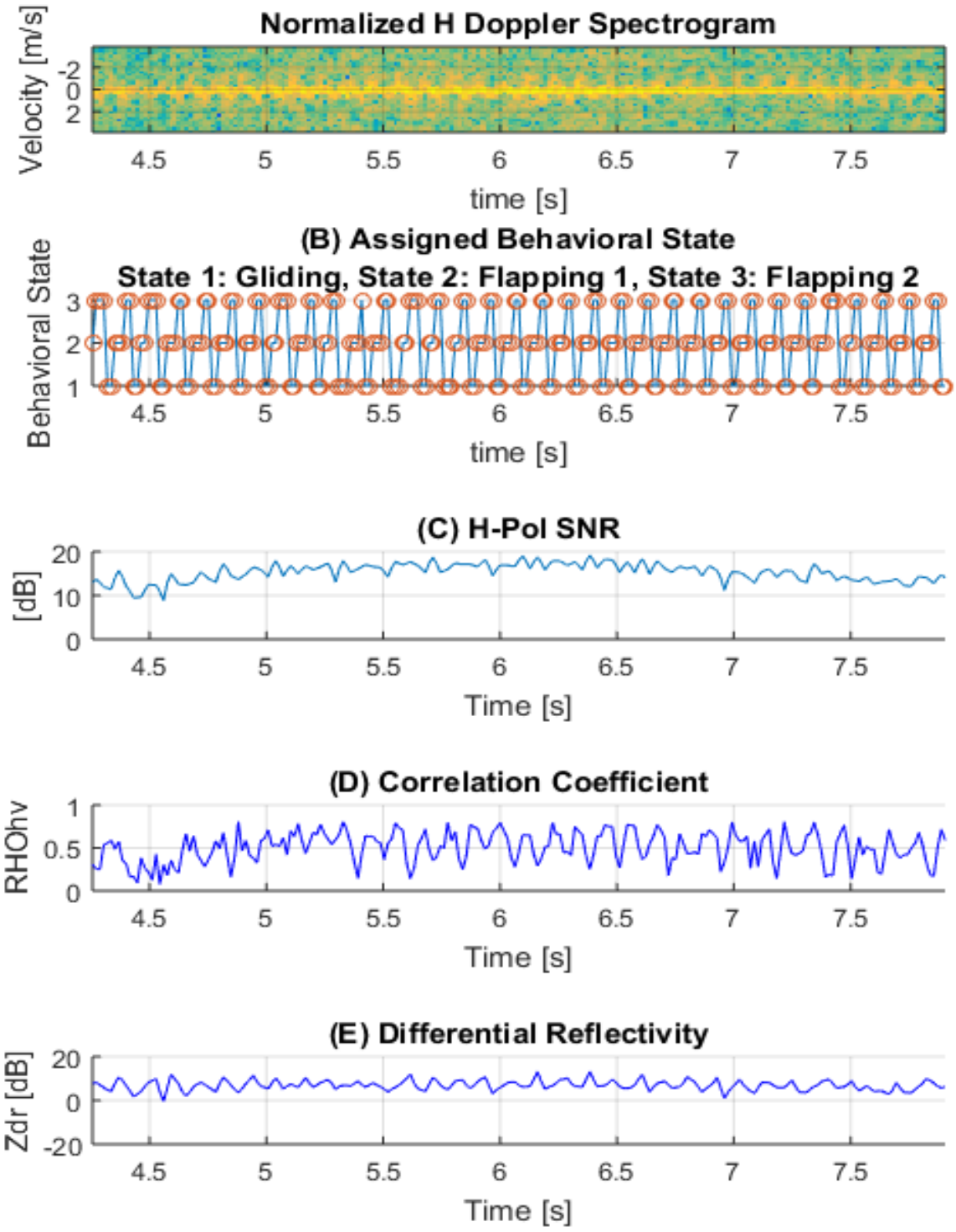

Figure 21 – This bird detection, also shown in Figure 15, flaps continuously at a constant rate. (B) Behavioral clustering results successfully capture this temporal information. (A)(C)(D), and (E) contain time-series measurements for reference.

A third example, previously discussed in Chapter 4 Figure 15, is included in Figure 21. This particular bird continuously flaps at a constant frequency. When this occurs, *State 1: Gliding* refers to the part of the flapping cycle with high correlation coefficient, rather than extended periods of gliding behavior. The physical meaning of these three states, in the context of the birds flight mechanics, requires further investigation with ground truth. For now, the objective is to ensure that all three states are correctly identified in a way that renders them comparable to other bird detections.

The k-means clustering algorithm does not independently assign a meaningful identity to the three clusters; it merely picks centroids that satisfy Eq. 4.1. In order to ensure that assigned behavioral states are both (A) physically meaningful and (B) comparable between bird detections, identity was assigned to the k-means output clusters according to the following rules:

(1) Behavioral State 1, "Gliding": *if* there is a behavioral state that remains active for extended time intervals, then this state is the gliding state. If there is no state with extended active intervals, then the state with the highest average correlation coefficient is determined to be the gliding state**.**

(2) **Behavioral State 2, "Flapping: Type 1"**: is the state, of the remaining two, with the highest average value of spectral width in the vertically polarized channel[8].

(3) **Behavioral State 3, "Flapping: Type 2"** : is the state remaining after the first two have been assigned.

[8] Follow up work might reevaluate the second rule based upon ground truth.

These rules were selected based upon a review of features containing maximum variance across the sample as well as several radar observations with paired video footage of the corresponding bird in flight.

4.1.3 Ranking Features by Classification Utility

The features listed in Table 4 were compared for their classification utility to determine, which, if any were the most useful in assigning time steps to different behavioral states. Classification utility was determined using principal component analysis, isolating the features that contribute most to the directions of greatest variance in the data. Using this method, a classification utility score was produced for each feature, separately for each bird detection. To achieve a general sense for how each feature performs across all bird, these utility scores were averaged for all bird detections. Results of this process are summarized in Figure 22.

The spectrogram row corresponding to the torso speed is the most useful row in both spectrograms, although other rows close to the torso speed seem to contain a fair amount of information as well. Physically speaking, spectrogram rows near the center row $\bar{v}$ represent the return power from components of the bird that are moving with respect to the torso. For this reason, their utility in classifying a bird's behavioral state was expected. Horizontally and vertically polarized power, along with correlation coefficient, differential reflectivity, and vertically polarized spectral width are also among the most useful features.

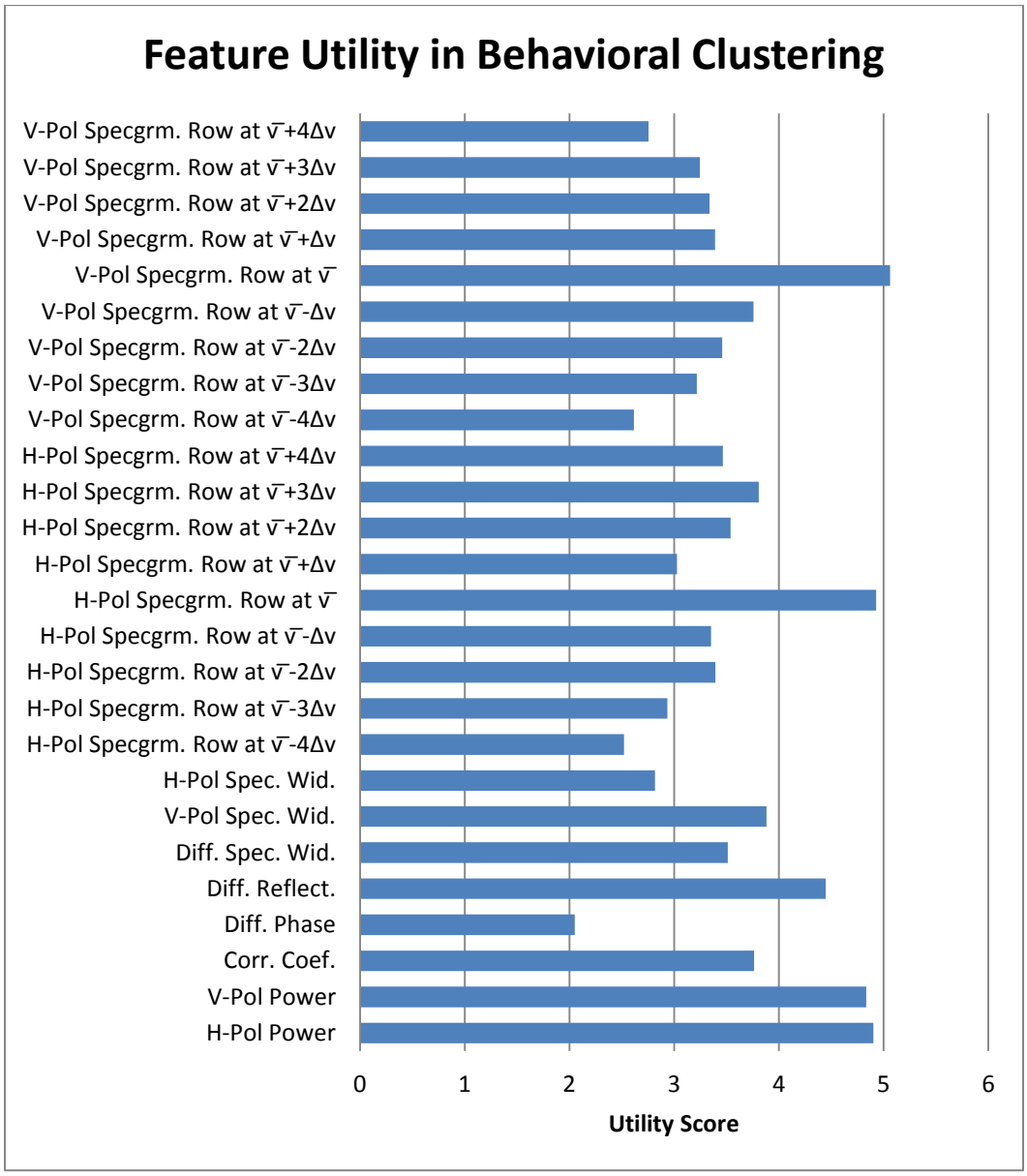

Figure 22 – Features are listed with a classification utility score, that indicates how useful they are in distinguishing between different behavioral states. Features with higher scores are more useful. Scores are averaged across the entire database of birds.

Finally it should be noted that the table contains aggregate results averaged across all birds; although the most useful polarimetric and Doppler features did differ substantially between bird observations. Spectrogram rows close to the center Doppler bin $\bar{v}$ were universally useful in classifying behavioral state across all birds, while

features like correlation coefficient were extremely useful in a subset of observations and only moderately useful in the rest, as shown in Figure 23.

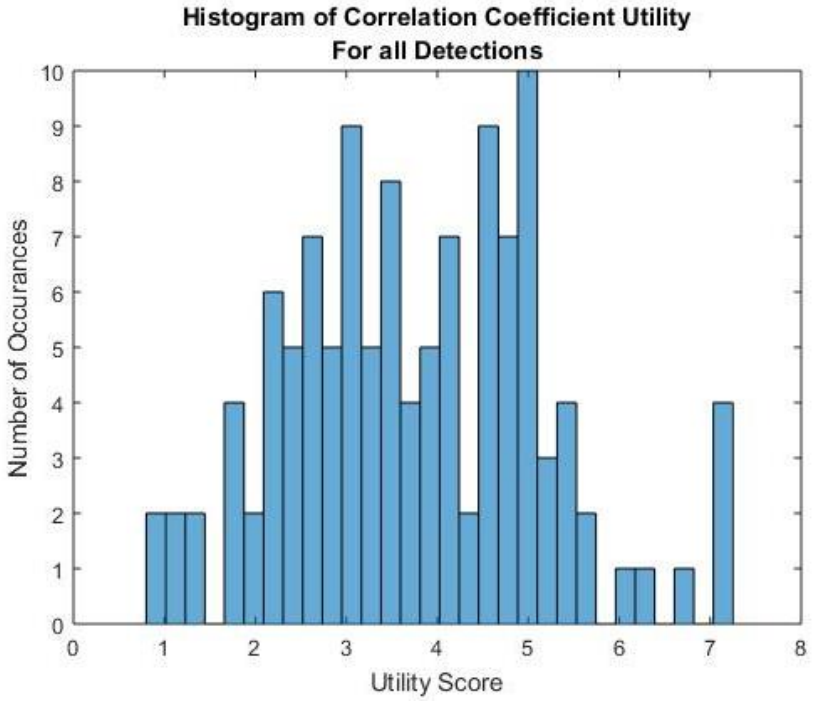

Figure 23 – Classification utility of certain features varied between bird detections; correlation coefficient is one example. Here, classification utility shows considerable spread, with an average score of about 3.75, as shown in Figure 22.

4.1.4 Improvement over Traditional Techniques

The method presented in this chapter maps a finite set of behavioral states to time-changing radar measurements. In the next chapter, an additional set of features will be extracted from these assigned behavioral states that enables comparison between birds. These features will be (A) temporal, describing the order and frequency of a birds different behaviors and (B) statistical, summarizing how each behavioral state generally looks to the radar.

These temporal and statistical features would not be possible without the *localized* information provided by the behavioral clustering technique. As discussed earlier,

conventional Fourier transform based methods for extracting wingbeat frequency and gliding intervals do not provide the same localized information and would perform poorly on some of the examples discussed in Section 6.2. In addition to serving as the basis for a second feature space (Chapter 7), localized behavioral state information may have other applications. For example, a kalman filter based tracker might adaptively update its kinematics model based upon the current behavioral state.

4.2 Feature Extraction Stage Two: Deriving the Second Feature Space From Behavioral States

Once the time-changing behavioral state of all birds has been determined, this information was used to produce a second set of features. This feature space enables meaningful comparison between different bird detection. Two types of features were generated for this purpose:

(1) **Temporal Features** – these describe the timing information contained in the assigned behavioral states. One classical temporal feature is wingbeat frequency.

(2) **Statistical Features** – these summarize how the bird appears to the radar during each of its behavioral states. The average value of correlation coefficient during gliding behavior is one statistical feature.

K-means clustering was applied to the collection of bird detections, sorting them into groups based upon their temporal and statistical features. Methods used to extract temporal and statistical features will be discussed in Sections 4.2.1 and 4.2.2 respectively.

4.2.1 Temporal Features

Mapping a behavioral state to each time step, as discussed in Chapter 6, provides a considerable amount of timing information. The duration, regularity, and order of each behavioral state are contained in these time series. Physically meaningful temporal features that are extracted from this information include:

(1) Average gliding duration, $\bar{T}_g$

(2) Average flapping duration, $\bar{T}_f$

(3) Average wingbeat period, $\bar{T}_{wb}$

(4) Average flapping duty cycle, $\bar{\delta}_{gf}$

In order to calculate these metrics, each behavioral state was reduced to a series of 'on' and 'off' time intervals. T_{ON_SN} is a vector containing the lengths of all on-times for behavioral state N; T_{OFF_SN} contains off-times. This concept is illustrated for the second behavioral state, Flapping-Type 2, in Figure 24.

As mentioned in Chapter 6, some birds flap at a constant rate, without extended gliding periods. For these birds, the first behavioral state ("gliding") actually represents a portion of the flapping cycle. In order to differentiate between this case and the bird that alternates between flapping and extended gliding periods, the values in T_{ON_S1} are compared to a threshold. On-times that exceed the threshold are categorized as confirmed gliding time-segments and are stored in $T_{ON\_S1\_G}$. All times that do not exceed the threshold are considered to be a portion of the flapping cycle, and are stored in $T_{ON\_S1\_F}$. In Figure 25, the on-time interval marked by arrow B would be classified as confirmed gliding and stored in $T_{ON\_S1\_G}$. Time interval C would not pass the threshold and would be considered as part of the gliding cycle.

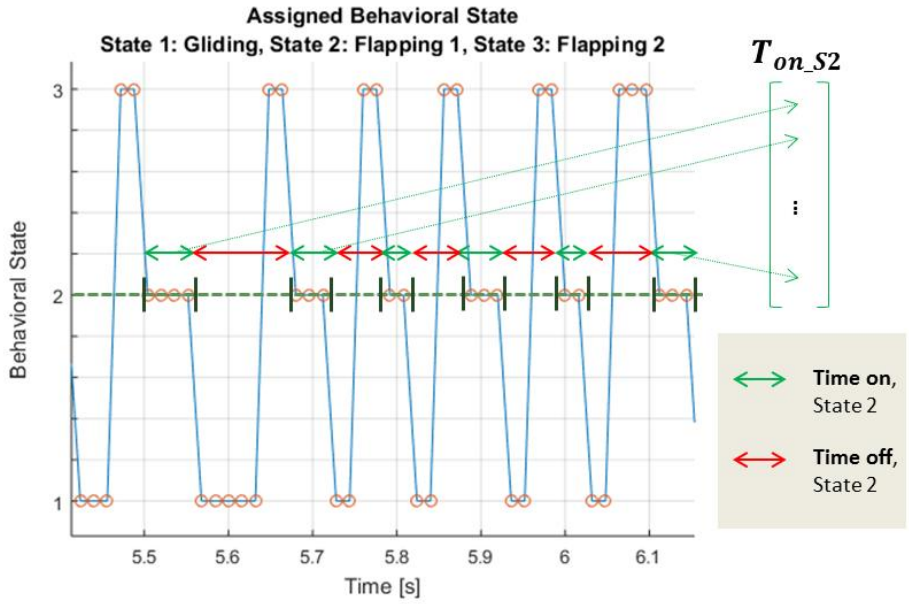

Figure 24 – Each behavioral state may be described as a series of consecutive "on" and "off" intervals. These on and of times are stored in T_{on_SN} and T_{off_SN} where N is the state number.

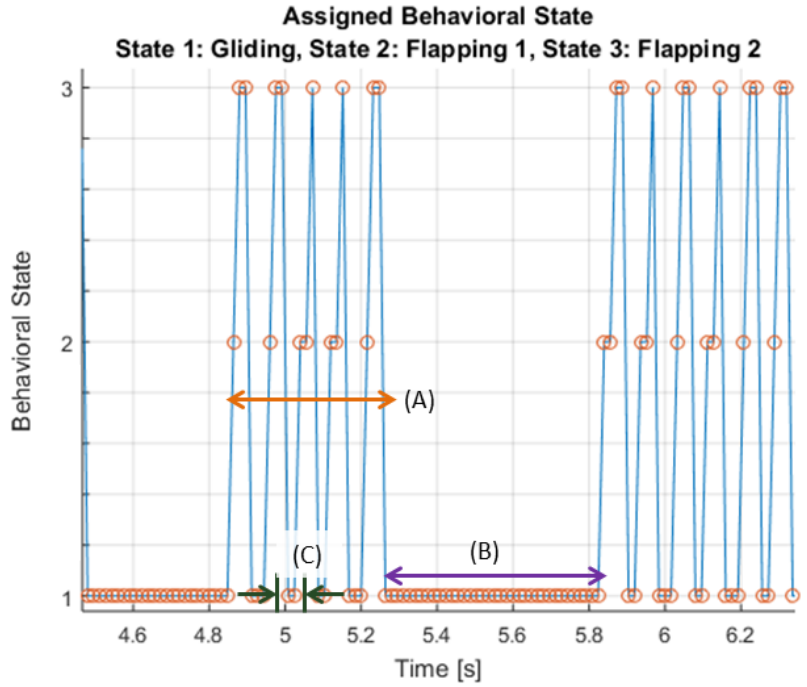

Figure 25 – Arrow (A) denotes a flapping interval T_f, arrow (B) marks an extended gliding period which would be stored in $T_{ON\_S1\_G}$, and (C) indicates an interval in T_{ON_S1} that would be considered as part of the flapping cycle and stored in $T_{ON\_S1\_F}$.

For birds where there are confirmed extended gliding intervals, the average gliding duration $\bar{T}_g$ is computed as:

$$\bar{\bar{T}}_g = mean(T_{ON\_S1\_G}) \tag{4.4}$$

For birds where there are no extended gliding intervals, with only continuous flapping, $\bar{T}_g$ is given by:

$$\bar{\bar{T}}_g = mean(T_{ON\_S1}) \tag{4.5}$$

Average flapping duration, $\bar{T}_f$, is computed as the average time interval between all consecutive time segments in $T_{ON\_S1\_G}$. In Figure 25, a single flapping interval T_f is indicated by arrow A. For birds that continuously flap, $\bar{T}_f$ is not computed.

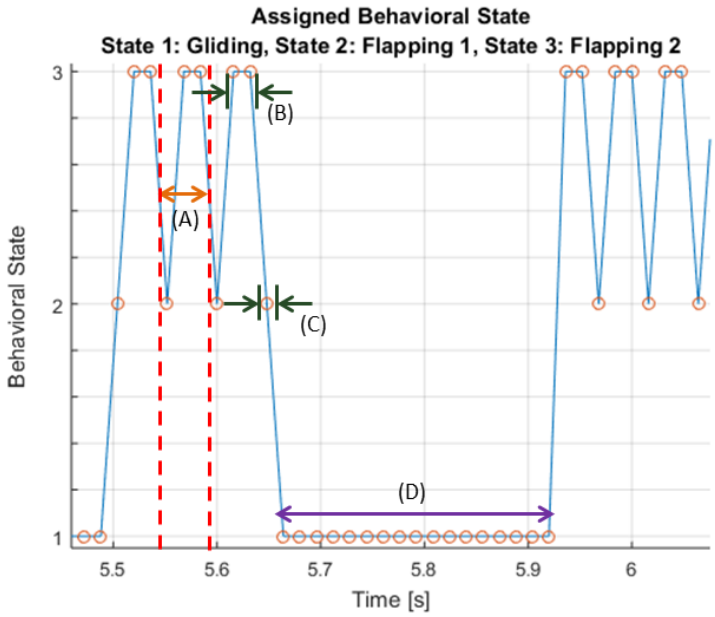

Figure 26 – Dashed red lines enclose a single wingbeat period (A). This period is the sum of time spent in State 2: Flapping Type 1 (C) and State 3: Flapping Type 2 (B)

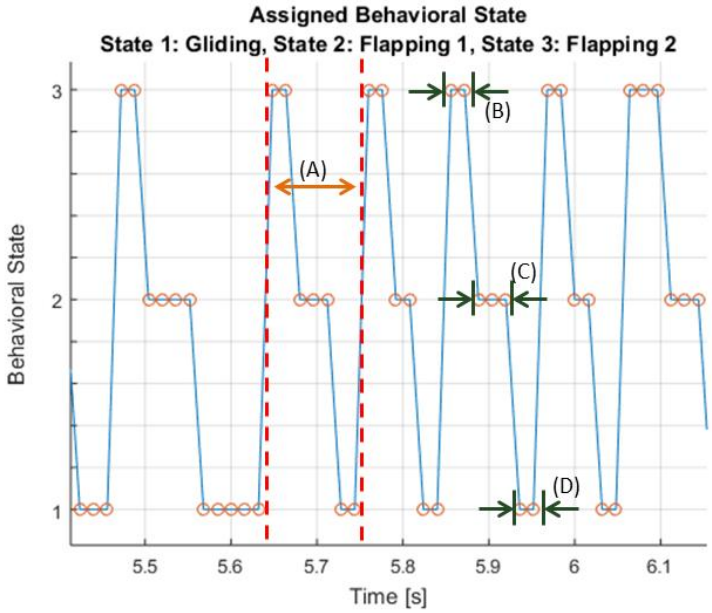

Figure 27 - Dashed red lines enclose a single wingbeat period (A). This period is the sum of time spent in State 1:Gliding (D), State 2: Flapping Type 1 (C) and State 3: Flapping Type 2 (B).

There are two different ways that the wingbeat period may present in terms of the behavioral state assignments. These two cases are shown in Figure 26 and Figure 27, where the region enclosed by dashed red lines indicates a single wingbeat period. The key difference is that the wingbeat period in Figure 26 does not include any time spent in behavioral state one; the wingbeat period in Figure 27 does. As a result, the wingbeat period in Figure 26 is the sum of time spent in state 2 (Flapping Type 1) and in state 3 (Flapping Type 2), labeled as intervals C and B respectively. To compute the *average* wingbeat period $\bar{T}_{wb}$ for this bird:

$$\bar{T}_{wb} = \overline{T_{ON\_S2}} + \overline{T_{ON\_S3}} \tag{4.6}$$

Likewise, the wingbeat period in Figure 27 is the sum of time spent in behavioral state 1 (Gliding), state 2 (Flapping Type 1), and state 3 (Flapping Type 2), shown as

intervals D, C, and B in the diagram. In this case, the average wingbeat period $\bar{T}_{wb}$, and wingbeat frequency f_{wb}, are given by:

$$\bar{T}_{wb} = \overline{T_{ON\_S1\_F}} + \overline{T_{ON\_S2}} + \overline{T_{ON\_S3}} \tag{4.7}$$

$$f_{wb} = 1/T_{wb} \tag{4.8}$$

Flapping duty cycle $\bar{\delta}_{gf}$ is the ratio of time spent gliding to the total time spent both flapping and gliding:

$$\bar{\delta}_{gf} = \frac{\bar{T}_g}{\bar{T}_f + \bar{T}_g} \tag{4.9}$$

For birds that only exhibit flapping behavior, $\bar{\delta}_{gf}$ is zero. In addition to the features listed above, the variances of $T_{ON\_S1\_F}$, $T_{ON\_S1\_G}$, T_{ON_S2}, and T_{ON_S3} were computed and used as features to describe the variability in a bird's temporal behavior.

4.1.2 Statistical Features

As described in Chapter 5, radar measurements change in time as birds cycle through different behavioral states. For example, gliding intervals are often associated with higher measured values of correlation coefficient. Because flight mechanics vary between different types of bird, corresponding measurement fluctuations contain useful species based classification information. When the behavioral state of a bird is known at each point in time, statistical properties of radar measurements may be analyzed *separately* for each behavioral state. In other words, all measurement values at time steps

assigned to the same behavioral state are considered together because, physically speaking, they all describe a similar measurement condition.

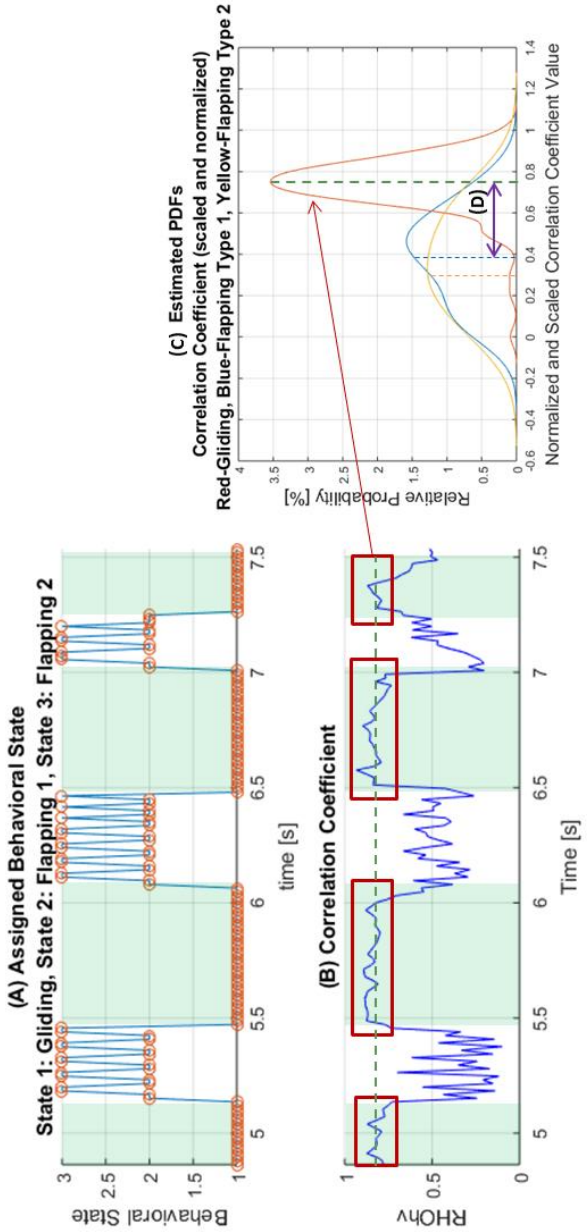

Figure 28 – Statistical features are calculated by considering measurement values that correspond to a given behavioral state together. Here, correlation coefficient is averaged *only* during gliding periods resulting in a higher, more representative, mean value. This mean value is a statistical feature, and so is the distance (D) between mean values for different behavioral states.

The method used for extracting statistical features is summarized visually in Figure 28. Here, the assigned behavioral state is shown at each step time, along with the corresponding correlation coefficient time series. Correlation coefficient is higher and less variable during assigned gliding intervals than during flapping periods. For this reason, accumulating statistics from the entire time series would result in poor features and a loss of meaningful information. Instead, each behavioral state is considered separately. The green shaded regions in Figure 28(A) and Figure 28(B) highlight gliding intervals, while red boxes enclose all measured values of ρ_{hv} at those times. These values may be accumulated into an estimated probability density function (PDF), shown in Figure 28(C). As expected this gliding PDF has a higher mean value and lower variance then the two flapping PDF's (yellow and blue).

The mean value and standard deviation of each PDF are considered to be statistical features that describe how this bird looks to the radar in terms of measurement ρ_{hv}, during each behavioral states. The mean value and standard deviation of measurement x in behavioral state n are named according to the following convention: μ_{sn_x} and σ_{sn_x}. In Figure 28, the distance between the PDF means for State 1 and State 2, $\mu_{s1\_\rho_{hv}} - \mu_{s2_{\rho_{hv}}} = \Delta_{\mu 12\_\rho_{hv}}$, marked by arrow (D), is an additional statistical feature. This metric describes how different ρ_{hv} measurement values tend to be between behavioral states. There are three of these features for each measurement; one for each PDF pair.

Statistical features μ_{sn_x}, σ_{sn_x}, and $\Delta_{\mu nm\_\rho_{hv}}$ were calculated for all behavioral states, across all measurements. Both scaled measurements, shown in Figure 18(C), and

unscaled measurements were used to produce statistical features, although scaled measurements were found to produce the most useful features.

CHAPTER 5

PRELIMINARY CLUSTERING RESULTS

The stated objective of this thesis is to analyze radar echoes for species based differences; the features described in Chapter 4 enable this type of analysis. Before performing clustering, imperfect detections were removed from the data set. These included any detections with multiple radial tracks, detections that had extreme radial acceleration (orientation change), and those not exceeding a predefined signal-to-noise threshold. After this down selection process, 152 detections remained in the dataset. This chapter will first attempt to validate the behavioral clustering method by comparing temporal trends observed in the data with established trends in bird flight behavior in Section 5.1. Next, select preliminary clustering results will be reviewed in Section 5.2. Section 5.3 will discuss the limitations of the data and future research directions.

5.1 Feature Extraction Validation and General Trends

Prior to performing clustering of birds, the dataset was evaluated against known bird flight characteristics to validate the behavioral clustering feature extraction method discussed in Chapter 4. Figure 29 shows a scatter plot comparing gliding interval with wingbeat frequency. Blue points represent birds that were not found to have a distinct gliding period during the feature extraction procedure; red dots indicate birds that alternate between flapping and gliding behaviors. As mentioned previously, for birds that

do not have an extended gliding interval, the gliding interval instead measures a portion of the flapping cycle.

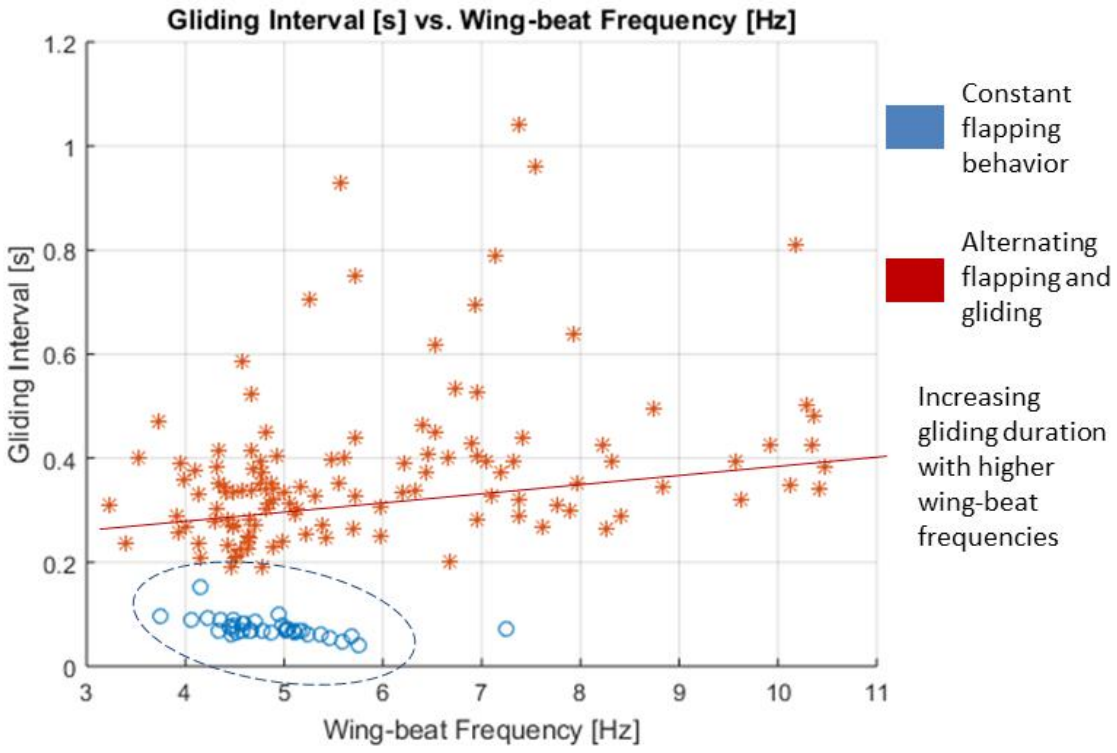

Figure 29 – Birds that alternate between flapping and gliding, shown in red, generally exhibit increasing wing-beat frequencies when the gliding period is longer. Wing-beat frequencies span 3-11Hz, which corresponds to results in published ecological research [13].

It is clear from the graph that the birds measured in this study had wing-beat frequencies spread between 3Hz and 11Hz. These values correspond almost exactly to standard wingbeat frequencies represented in Table 3. This plot also shows an interesting trend of increasing wing-beat frequency with increasing gliding period. Although I could not find a corresponding pre-established trend supporting this finding, it makes intuitive physical sense; if two birds of the same species have different gliding periods, the individual gliding for longer intervals would need to exert more energy during its flapping period to maintain the same flight performance. Finally, it should be noted that

both groups depicted in Figure 29 may contain species based sub-groups. The red flapping and gliding group appears to have at least two sub-clusters of points. Division within this group will be further explored in Section 5.1, although this type of analysis will ultimately require a larger dataset.

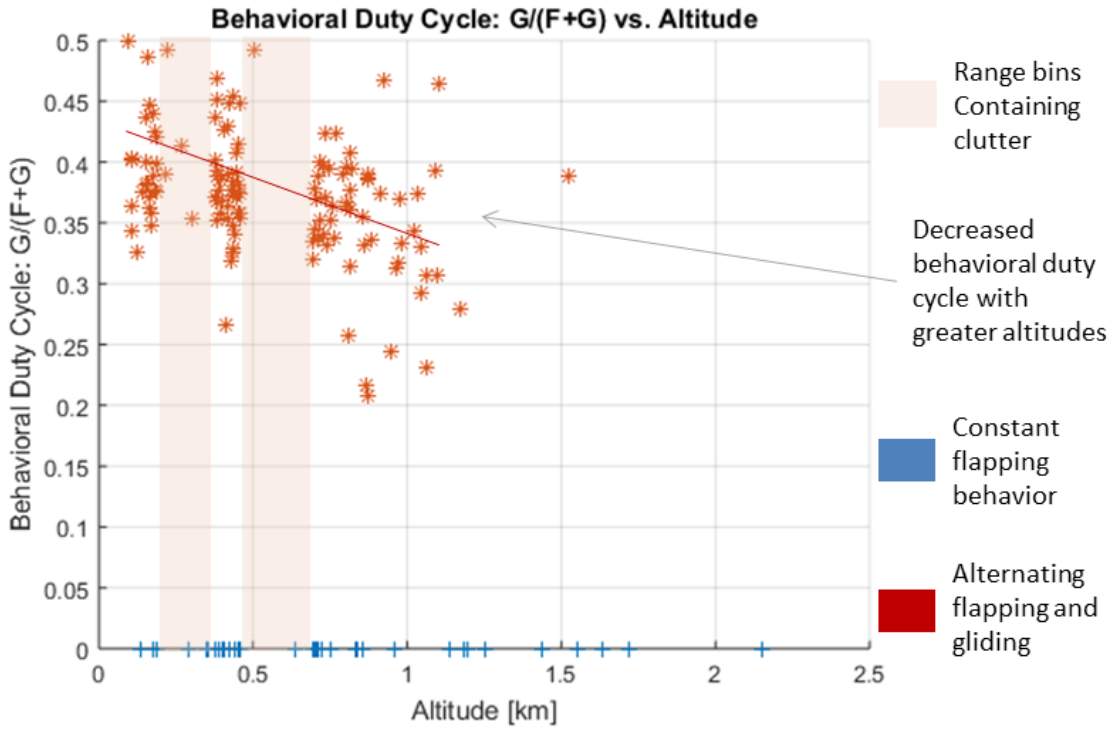

Figure 30 – Birds that had no extended gliding period have a behavioral duty cycle of zero, and are shown in blue. Birds that alternate between flapping and gliding behaviors generally spend less time gliding at higher altitudes. Pink columns indicate altitudes with fewer detections due to ground clutter. Ground clutter appears in antenna sidelobes, and not at the actual altitude indicated in the image.

Figure 30 and Figure 31 show the same two groups of birds, plotted against their measured altitude. In both figures, two pink shaded regions indicate ranges that had substantial ground clutter returns. Due to the clutter, these regions had fewer viable bird detections. In Figure 30, behavioral cycle, or the ratio of time spent gliding to all other behaviors, is shown to decrease with increasing altitude (i.e. shorter gliding periods).

Similarly, Figure 31 illustrates an apparent increase in wing-beat frequency with greater altitude measurements. This measurement is supported by previous Ecological research, which has already correlated altitude with both changing flight behavior and with the presence of different species of bird altogether. Thinner air has been associated with a necessary increase in wingbeat frequency. It is also known that, as birds ascend during migration, they flap faster and pick up speed [15]. To my knowledge, the correlation between altitude and shorter gliding periods has not been previously observed, however this trend may occur for the same reasons as increased wingbeat frequency.

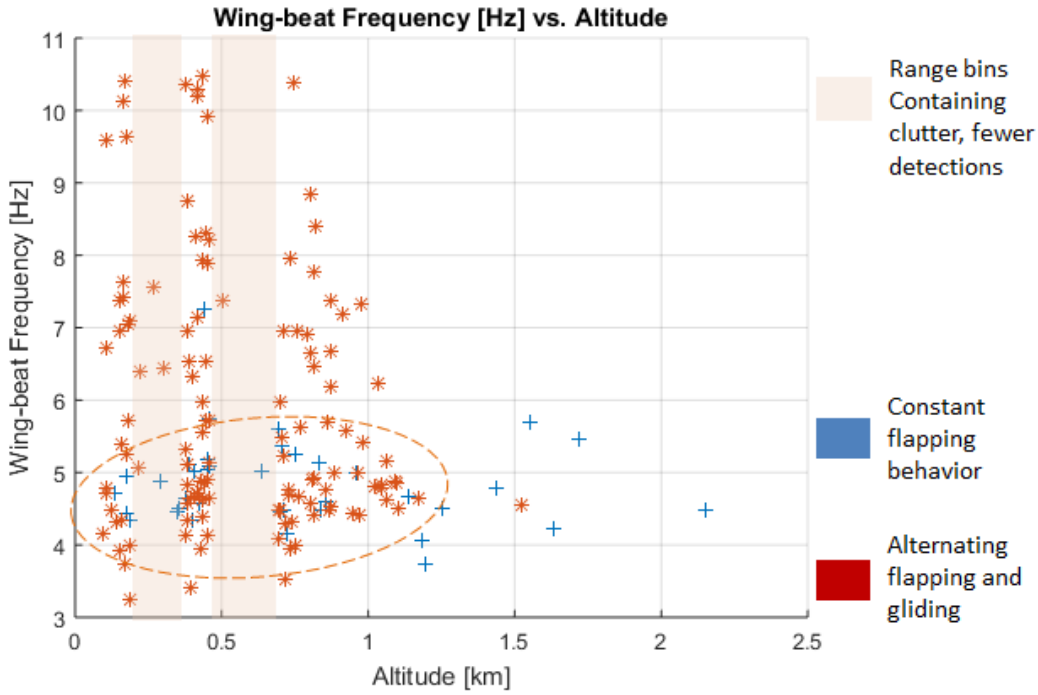

Figure 31 – Birds without an extended gliding period are shown in blue; birds that alternate between flapping and gliding are shown in red. The flapping and gliding group may have three potential subgroups, the bottom one is circled. A general trend towards higher wing-beat frequencies with greater altitudes is observed. Pink regions mark altitudes that contain fewer detections due to clutter.

Generally speaking, the temporal information, extracted from each bird detection using the behavioral clustering method, was found to match published Ecological

research. Specifically, the trend towards greater wingbeat frequencies at greater altitudes, as well the span of measured wing-beat frequencies, strongly match the literature. Other measured trends, such as the positive relationship between gliding interval and wingbeat frequency, make sense from a physical perspective, considering the dynamics of a bird in flight. Together, these findings strongly support the performance of the behavioral clustering feature extraction method as a tool for producing temporal/behavioral information.

5.2 Other Clustering Results

As shown in Section 5.1, temporal features enable us to immediately divide bird observations into groups of birds that only flap and those that both flap and glide. These groups show considerable variance across the different temporal features, as shown for wingbeat frequency and gliding interval in Figure 29. It is fully expected that both groups contain a number of different species. A logical approach to evaluate the species-based classification potential of the statistical features might involve looking deeper into groups of observations that have similar *temporal* characteristics, such as the two groups in Figure 29. Because this is an unsupervised dataset, and features vary with both orientation and species, it makes sense to start the analysis within groups defined by features that are already known to have a species-based dependence. A group of detections that share temporal characteristics represent a subset of the total species contained in the data. Looking within just this group simplifies the problem and allows us to hopefully isolate species and orientation based trends.

Unfortunately, as mentioned previously, the filtered dataset contained a total of 152 bird detections. While this is more than enough to establish general trends, it is not sufficient to perform the analysis described about. There are simply not enough birds that only flap, for example, to establish any species based trends within this group. However, preliminary results are promising.

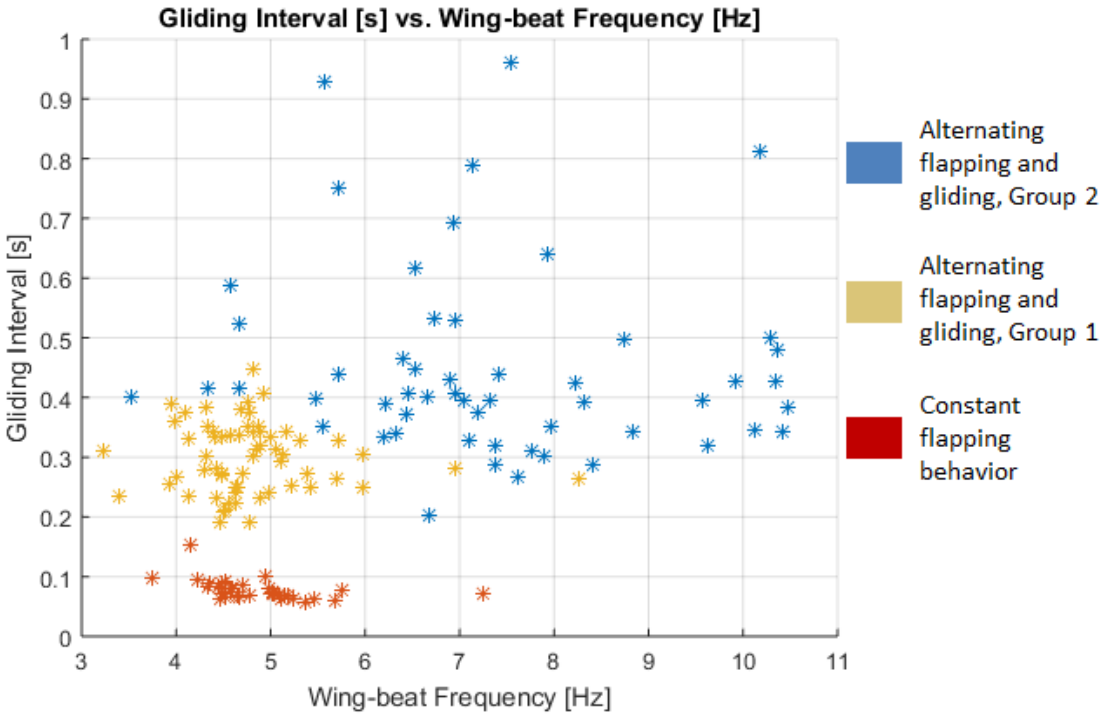

Figure 32 – Bird detections were clustered into three groups, based solely on their temporal features.

Figure 32 shows the collection of detections divided into 3 groups, using k-means clustering, based solely on equally weighted temporal features. One group mostly

exhibits constant flapping behavior[9], the other two alternate between flapping in gliding but generally span different wingbeat frequencies. These groups were evaluated in terms of the statistical features and select results are shared below.

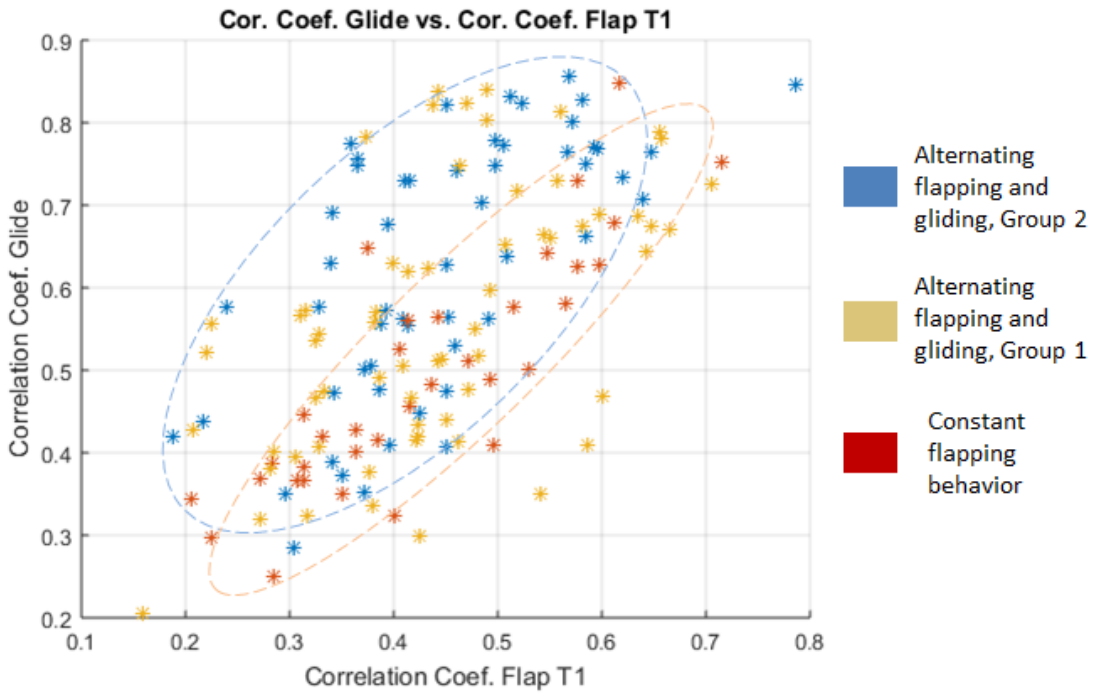

Figure 33 – Groups of birds with similar temporal characteristics have different spreads of correlation coefficient during flapping and gliding periods

Figure 33 shows the same three clusters, plotted in terms of their measured correlation coefficient. Here, the y-axis represents correlation coefficient measured during gliding behavior; the x-axis is correlation coefficient during flapping behavior (Type 2). Although there is some overlap, the blue group, which was the flapping and gliding cluster with higher wingbeat frequencies, generally has higher correlation coefficient then the other two groups while flapping.

[9] The red group is not exclusively birds that had no gliding intervals. There are also some birds with very short flapping intervals in this group. It is named for ease of reference.

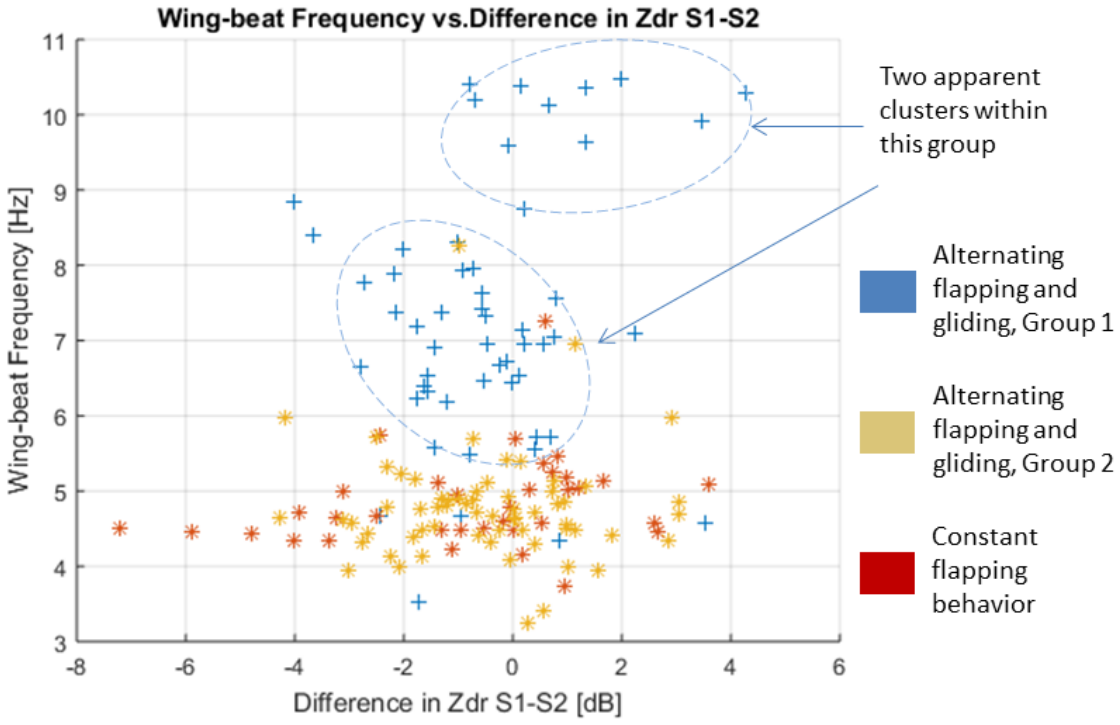

Figure 34 – The blue group, birds that alternate between flapping and gliding and have higher wingbeat frequencies, appears to have two sub-clusters, marked by arrow. These groups exhibit different wingbeat frequency as well as larger differences in differential reflectivity in flapping and gliding states.

Figure 34, again, shows the same three clusters. Here, they are plotted in terms of wingbeat frequency and difference in differential reflectivity between flapping and gliding states. This plot shows two subgroups within the blue group that have different spreads of the differential reflectivity metric and that are also separated in wingbeat frequency. Although more data is needed to support this finding, it indicates that there are meaningful subgroups within groups of birds that share temporal features in common. It is certainly possible that these two subgroups represent orientation differences. However, this is likely not the case due to the difference in wingbeat frequency. Also, the difference between differential reflectivity during flapping and gliding states measures the degree to

which a birds aspect ratio changes, with respect to the radar, as it alternates between flapping and gliding states. This could easily be a species dependent metric because wing cross-section, and orientation during flapping, are a function of species.

5.3 Limitations and Future Work

Based upon the findings presented in this chapter, it is clear that the behavioral clustering method yields viable temporal information. To an extent, this temporal information has already been associated with species [13]; however this thesis presented and validated a novel technique for extracting it from echoes in a more localized and robust way. The size of the dataset was a limiting factor in providing an extensive analysis of some of the statistical features. However, two examples of potential species based clusters were shown in Section 5.2.

With a more extensive dataset, birds that share temporal qualities could be isolated and analyzed separately for species-based subgroups. Within these groups, statistical features may be evaluated for orientation dependence, using the radial velocity as a rough estimate. The orientation dependence of biological scatterers is established [8]. If the orientation profile can be characterized, it may be an advantage in a future classification algorithm. With a larger dataset, the tools now exist to begin this process.

As shown, there is a considerable amount of variance in the data. However, most of the information is contained in the way that measurements change in time with respect to themselves and other measurements. Using the tools presented above, and a larger dataset, this variation could be characterized and mapped to broad species based groups.

CHAPTER 6

SUMMARY AND CONCLUSION

The stated objective of this thesis was to evaluate features for species based classification potential. Towards this objective, a novel feature extraction technique and preliminary clustering results of a set of bird detections were presented. While initial results were promising, further research, with a larger set of detections and corresponding ground truth, are needed to confirm that species based differences exist.

The behavioral clustering technique described in Chapter 4, and validated in Chapter 5, is a viable alternative to conventional Fourier based methods for extracting wingbeat frequency and other temporal characteristics. Behavioral clustering yields more localized frequency information and works for shorter duration detections. In addition, because this method determines behavioral state using many simultaneous measurements, it is more robust. Knowledge of instantaneous behavioral state could also be useful in other applications. For instance, it may allow for an adaptable tracking algorithm that updates its kinematic model based upon the current behavior.

When behavioral state is known, this information may be translated into statistical and temporal features that provide a holistic description of the bird. These features showed variance across the sample, and groups of birds that had similar temporal characteristic were found to contain potential subgroups with different statistical features. However, the size of the dataset limited the extent of the analysis that could be performed. The tools presented in this thesis may be used for further analysis on a larger dataset to uncover species and azimuthal based trends.

BIBLIOGRAPHY

[1] T. H. Kunz, E. B. Arnett, B. Cooper, P. W. Erickson and P. R. Larkin, "Assessing impacts of wind-engery development on nocturnally active birds and bats: a guidance document," *Journal of Wildlife Management,* vol. 71, no. 8, pp. 2449-2486, 2007.

[2] P. B. Chilson, "Partly cloudy with a chance of migration: weather, radars, and aeroecology," *Bull. Amer. Meteor. Soc.*, vol. 93, no. 5, pp. 669-686, 2012.

[3] S. Bachmann and D. Zrnic, "Spectral density of polarimetric variables separating biological scatterers in the VAD display," *Journal of atmospheric and oceanic technology,* vol. 24, no. 7, pp. 1186-1198, 2007.

[4] S. Bachmann and D. Zrnic, "Three-dimensional attributes of clear-air scatterers observed with the polarimetric weather radar," *IEEE geoscience and remote sensing letters,* vol. 5, no. 2, p. 231, 2008.

[5] V. Melnikov and M. Leshkinen, "Doppler velocities at orthogonal polarizations in radar echoes from insects and birds," *IEEE geoscience and remote sensing letters,* vol. 11, no. 3, p. 592, 2014.

[6] M. Van Den Broeke, "Polarimetric radar observations of biological scatterers in hurricanes irene (2011) and sandy (2012)," *Journal of atmospheric and oceanic technology,* vol. 30, no. 12, pp. 2754-2767, 2013.

[7] P. Stepanian, "Ph.D thesis: Radar polarimetry for biological applications," The University of Oklahoma, Norman, 2015.

[8] P. Stepanian and K. Horton, "Extracting migrant flight orientation profiles using polarimetric radar," *IEEE transactions on geoscience and remote sensing,* pp. 1-11, 2015.

[9] D. Zrnic and A. Ryzhkov, "Observations of insects and birds with a polarimetric radar," *IEEE transactions on geoscience and remote sensing,* vol. 36, no. 2, pp. 661-668, 1998.

[10] C. Vaughn, "Birds and insects as radar targets: A review," *Proceedings of the IEEE,* vol. 73, no. 2, pp. 205-227, 1985.

[11] B. Bruderer, P. Dieter, A. Boldt and F. Liechti, "Wing-beat characteristics of birds recorded with tracking radar and cine camera," *Internation journal of avian science,* vol. 152, no. 2, pp. 272-291, 2010.

[12] V. Venkatesh, "The UMass X-Pol mobile Doppler radar: description, recent observations, and new system developments," in *Geoscience and remote sensing symposium, 2008. IGARSS 2008. IEEE international.*, Boston, MA, 2008.

[13] C. J. Pennycuick, "Wingbeat frequency of birds in steady cruising flight: new data and improved predictions," *The journal of experimental biology,* vol. 199, no. 7, pp. 1613-1618, 1996.

[14] W. k. Pratt, Digital Image Processing, 2nd ed., New York: John Wiley & Sons, 1991.

[15] H. Schmaljohann and F. Liechti, "Adjustments of wingbeat frequency and air speed to air density in free-flying migratory birds," *The journal of experimental biology,* pp. 3633-3642, 2009.